Int J Geomath (2015) 6:1–42
DOI 10.1007/s13137-015-0070-z

ORIGINAL PAPER

Signal analysis via instantaneous frequency estimation of signal components

Charles K. Chui · Maria D. van der Walt

Received: 29 January 2015 / Accepted: 12 February 2015 / Published online: 25 February 2015

Abstract The empirical mode decomposition (EMD) algorithm, introduced by Huang et al. (Proc Roy Soc Lond Ser A Math Phys Eng Sci 454(1971):903–995, 1998), is arguably the most popular mathematical scheme for non-stationary signal decomposition and analysis. The objective of EMD is to separate a given signal into a number of components, called intrinsic mode functions (IMF's) after which the instantaneous frequency (IF) and amplitude of each IMF are computed through Hilbert spectral analysis (HSA). On the other hand, the synchrosqueezed wavelet transform (SST), introduced by Daubechies and Maes (Wavelets in Medicine and Biology, pp. 527–546, 1996) and further developed by Daubechies et al. (Appl Comput Harmon Anal 30:243–261, 2011), is applied to estimate the IF's of all signal components of the given signal, based on one single reference "IF function", under the assumption that the signal components satisfy certain strict properties of a so-called adaptive harmonic model, before the signal components of the model are recovered. The objective of our paper is to develop a hybrid EMD-SST computational scheme by applying a "modified SST" to each IMF of the EMD, as an alternative approach to the original EMD-HSA method. While our modified SST assures non-negative instantaneous frequencies of the IMF's, application of the EMD scheme eliminates the dependence on a single reference IF value as well as the guessing work of the number of signal components in the original SST approach. Our modification of the SST consists of applying vanishing moment wavelets (introduced in a recent paper by C.K. Chui, Y.-T. Lin and H.-T. Wu)

C. K. Chui
Department of Statistics, Stanford University, Stanford, CA 94305, USA
e-mail: ckchui@stanford.edu

M. D. van der Walt (✉)
Department of Mathematics and Computer Science, University of Missouri-St. Louis, St. Louis, MO 63121, USA
e-mail: maryke.thom@gmail.com

with stacked knots to process signals on bounded or half-infinite time intervals, and spline curve fitting with optimal smoothing parameter selection through generalized cross-validation. In addition, we formulate a local cubic spline interpolation scheme for real-time realization of the EMD sifting process that improves over the standard global cubic spline interpolation, both in quality and computational cost, particularly when applied to bounded and half-infinite time intervals.

Keywords Time–frequency analysis · Instantaneous frequency · Empirical mode decomposition · Intrinsic mode functions · Synchrosqueezing wavelet transform · Hilbert transform · Hilbert spectrum · Adaptive harmonic model · Local spline interpolation

Mathematics Subject Classification 94A12 · 41A05 · 41A15

1 Introduction

Time–frequency analysis is one of the most important and powerful mathematical tools for data analysis, understanding, visualization, and manipulation, when the data may change with the time variable (as in signal processing and time series analysis), the spatial variables (as in digital image compression and manipulation), or both time and spatial variables (as in the study of heat diffusion, vibrating strings or membranes, seismic waves, and digital videos). The study of time–frequency analysis originates from quantum mechanics in the late 1920s. In the development of its mathematical foundation, Werner Heisenberg stated in his 1927 paper (Heisenberg 1927) that "the more precisely the position (of an elementary particle) is determined, the less precisely the momentum is known in this instant, and vice versa". In the following year, two mathematicians, Earle Kennard and Hermann Weyl, independently derived the precise lower bound of this "position-momentum measurement", called the *Heisenberg uncertainty principle* (Kennard 1927; Weyl 1928). In the language of time–frequency analysis, this principle is a restriction for simultaneous time–frequency localization of a (finite-energy) signal. More precisely, when the Plancherel identity is applied to the windowed Fourier transform (commonly called short-time Fourier transform, STFT, in the signal processing literature), the area of the time–frequency localization window (in the time–frequency plane) is bounded below precisely by 2, when the standard deviation of the (one-variable) window function is used for the STFT.

In his 1946 pioneering paper (Gabor 1946) on the mathematical theory of communications, Dennis Gabor used the Gaussian function

$$g_\sigma(x) = \frac{1}{2\sigma\sqrt{\pi}} e^{-\left(\frac{x}{2\sigma}\right)^2}$$

as the window function to achieve the uncertainty lower bound, introducing the Gabor transform by choosing $\sigma = \frac{1}{2\sqrt{\pi}}$. In the course of this investigation, Gabor also introduced the notion of the *complex signal extension* $f^\star$ (commonly called *analytic signal extension* in the current signal processing literature) of a given real-valued function f, defined by

$$f^\star(t) = f(t) + i(\mathcal{H}f)(t), \quad t \in \mathbb{R}, \tag{1}$$

where $\mathcal{H}$ denotes the Hilbert transform; that is, the Cauchy principal value of the convolution over $\mathbb{R}$ with integral kernel $\frac{1}{\pi t}$. Hence, by taking the real part of the polar formulation of $f^\star$, the given function f has the representation

$$f(t) = A(t)\cos 2\pi\phi(t), \tag{2}$$

where $A(t)$ and $\phi(t)$, called the amplitude and phase of f, respectively, are given by

$$A(t) = |f^\star(t)| \quad \text{and} \quad \phi(t) = \frac{1}{2\pi}\tan^{-1}\frac{(\mathcal{H}f)(t)}{f(t)}. \tag{3}$$

In the same volume of the IEE journal where (Gabor 1946) appeared, Van der Pol (1946) arrived at this same representation of $f(t)$ in (2)–(3), by considering the simple harmonic motion. Since a mono-tone signal $f_1(t)$ with frequency ω_1 Hz (where Hz stands for the unit *Hertz*, for measuring the number of cycles of oscillation per second, when t is considered as the time variable) can be formulated as

$$f_1(t) = a_1\cos 2\pi\omega_1 t, \tag{4}$$

for some positive constant a_1, it is natural to define the so-called *instantaneous frequency* (IF) of f in (2) by the derivative $\phi'(t)$ of its phase function $\phi(t)$. But is this an acceptable definition for time–frequency representation of an arbitrary signal with time domain $\mathbb{R}$? More recently, there have been other attempts to define instantaneous frequency, particularly in the early 1990s, with the most successful ones based on the Wigner–Ville distribution method (see, for instance, Boashash 1992a, b). It is noted, however, that all such studies share the same characteristics as the pioneering work of Gabor and Van der Pol, in that only one frequency value of a given function f is considered.

To address the above question, let us turn to the early study of partial differential equations (PDE's) in the "golden" period, shortly after the 1687 publication of Sir Isaac Newton's *Principia*, which is arguably the greatest mathematical treatise since Euclid's *Elements*. During their five-year collaboration between 1727 and 1732 at the St. Petersburg Academy of Sciences, Daniel Bernoulli and Leonhard Euler accomplished an incredible amount of important pioneering work, particularly in areas of hydrodynamics, theory of oscillations, political economics, and probability theory. Therefore, it is surprising to learn that even these two mathematical giants could not agree on the solution of the vibrating string PDE, described by

$$\begin{cases} \frac{\partial^2}{\partial t^2}u(x,t) = c^2\frac{\partial^2}{\partial x^2}u(x,t), & 0 \le x \le L,\ t \ge 0; \\ u(x,0) = u_0(x), & 0 \le x \le L, \end{cases} \tag{5}$$

where c is a positive constant and $u_0(x)$ is a continuous function on the interval $[0, L]$ that describes the initial displacement of the string. Bernoulli proposed that the solution should be the infinite series

$$u(x,t) = u_0(0) + \sum_{k=1}^{\infty} b_k \sin\left(\frac{k\pi x}{L}\right)\cos\left(\frac{ck\pi t}{L}\right), \tag{6}$$

for some constants b_k, $k = 1, 2, \ldots$. It is clear that the expression of $u(x,t)$ in (6) satisfies the PDE in (5), at least formally, but Bernoulli could not formulate the coefficients b_k in terms of the initial displacement function $u_0(x)$. It should be pointed out that this remarkable discovery by Bernoulli was more than 50 years before Joseph Fourier introduced the concept of Fourier series. However, Euler thought that Bernoulli's proposed solution was absurd, pointing out that it excludes any initial displacement function $u_0(x)$ with $u_0(L) \neq u_0(0)$. Euler then proposed his own solution:

$$u(x,t) = \frac{1}{2}\left(u_0(x+ct) + u_0(x-ct)\right). \tag{7}$$

Of course, both Bernoulli and Euler were correct, and their solutions are actually identical. This can be easily justified by using the Fourier series expansion of the odd function extension of $u_0(x) - u_0(0)$, namely

$$u_0(x) = u_0(0) + \sum_{k=1}^{\infty} b_k \sin\left(\frac{k\pi x}{L}\right), \quad -L \le x \le L. \tag{8}$$

Indeed, while the solution (6) of Bernoulli can be obtained by applying the current standard method of separation of variables in PDE, Euler's solution (7) yields the same formulation as (6) when the Fourier sine series representation in (8) of u_0 is used in (7), with x in (8) replaced by $x + ct$ and by $x - ct$, respectively.

Returning to Bernoulli's solution, observe that, for any fixed $x \in [0, L]$, the infinite series (6) is an example of the general Fourier cosine series

$$f(t) = \frac{1}{2}c_0 + \sum_{k=1}^{\infty} c_k \cos\left(\frac{2\pi kt}{T}\right), \quad -\frac{T}{2} \le t \le \frac{T}{2}, \tag{9}$$

with $T = \frac{2L}{c}$, $f(t) = u(x,t)$, $c_0 = 2u_0(0)$, and $c_k = b_k \sin\left(\frac{k\pi x}{L}\right)$, $k = 1, 2, \ldots$. In addition, the mono-tone signal $f_1(t)$ in (4) is also a special case of the general signal in (9), with $a_1 = c_{k_0}$ for some $k_0 \geq 1$, $c_k = 0$ for $k_0 \neq k = 0, 1, \ldots$, and $\omega_1 = \frac{k_0}{T}$. In general, by considering the Fourier series of even function extensions, every finite-energy signal f on the bounded interval $[0, \frac{T}{2}]$ has a Fourier cosine series representation given by (9). Therefore, every periodic signal f, with period T as in (9), has frequencies $\omega_k = \frac{k}{T}$ for all positive integers k, provided that $c_k \neq 0$.

On the other hand, for a finite-energy signal f with time-domain $\mathbb{R}$, the Fourier transform is commonly used, instead, to study its frequency content. For the sake of mathematical elegance, let us consider the following formulation of the Fourier transform $g(\omega) := \hat{f}(\omega)$ and the corresponding inverse Fourier transform $\check{g}(t)$:

$$\begin{cases} g(\omega) = \hat{f}(\omega) := \int_{\mathbb{R}} f(t) e^{-i2\pi\omega t} \mathrm{d}t; \\ \check{g}(t) := \int_{\mathbb{R}} g(\omega) e^{i2\pi\omega t} \mathrm{d}\omega. \end{cases}$$

Recall that $\check{g} = f$ if $g \in L_1(\mathbb{R})$. Therefore, the Fourier transform of the *stationary signal*

$$f(t) = \sum_{k=1}^{K} a_k \cos 2\pi(\omega_k t + d_k) \tag{10}$$

is given by

$$\hat{f}(\omega) = \frac{1}{2} \sum_{k=1}^{K} a_k e^{i2\pi\omega d_k/\omega_k} \left(\delta(\omega - \omega_k) + \delta(\omega + \omega_k)\right),$$

for arbitrary frequency values $\omega_k > 0$ and real values d_k, where $k = 1, \ldots, K$, and δ denotes the Dirac delta distribution. We remark that the signal f in (10) is said to be stationary, since the frequencies ω_k, $k = 1, \ldots, K$, are independent of the time variable $t \in \mathbb{R}$. Hence, the frequencies of a stationary signal with time domain $\mathbb{R}$ can be easily determined by applying the Fourier transform (and, in practice, by the fast Fourier transform, FFT, followed by thresholding with a sufficiently large positive parameter).

We are now ready to address the question on the notion of instantaneous frequency, as discussed in the beginning of this section. For the stationary signal f defined by (10), since the Hilbert transform of the cosine function is the sine function, it follows from (1) that the analytic signal extension $f^\star$ of f is given by

$$f^\star(t) = \sum_{k=1}^{K} a_k e^{i2\pi(\omega_k t + d_k)},$$

which is called the *Hilbert spectrum* of the given signal f in the current signal processing literature. Unfortunately, while each ω_k, where $k = 1, \ldots, K$, is a frequency of f, provided that $a_k \neq 0$, the formulation of $f(t)$ in (2) with phase $\phi(t)$, resulting from the definition (3), only yields one instantaneous frequency $\phi'(t)$. Furthermore, if the stationary signal f in (10) is non-periodic (with the simple example: $K = 2$, $\omega_1 = 1$, $\omega_2 = \sqrt{2}$, $d_1 = 0$, $d_2 = 0$, $a_1 \neq 0$, and $a_2 \neq 0$ in [10)], the Fourier cosine series representation of f, as given by (9), necessarily introduces infinitely many non-zero frequencies $\frac{k}{T}$ for any choice of $T > 0$, where $k = 1, 2, \ldots$. In view of this discussion, without any restriction to a suitable signal model, it is a daunting task to give an acceptable definition of "instantaneous frequency" for an arbitrary signal, as an extension of the definition of frequencies for stationary signals, regardless of bounded or unbounded time intervals.

In this paper, we will consider the signal model *AHM*, which stands for the *adaptive harmonic model* (see Daubechies et al. 2011; Thakur and Wu 2011; Chui et al. 2014; Chui and Mhaskar 2015), defined by

$$\begin{cases} f(t) = \sum_{k=1}^{K} f_k(t) + T(t); \\ f_k(t) = A_k(t)\cos 2\pi\phi_k(t), \quad k = 1, \ldots, K, \end{cases} \tag{11}$$

where $T(t)$ is some polynomial (possibly embedded with noise), $A_k(t) \geq 0$, and $\phi_k(t) \in C^1$ with $\phi_k'(t) \geq 0$, for all t in the time interval, which may be bounded or unbounded. Observe that this is a natural extension of (2) and (10), from one signal component to an arbitrary number of components and from $\omega_k t + d_k$ to arbitrary C^1 functions $\phi_k(t)$, respectively. We will call $T(t)$ and $\phi_k'(t)$, $k = 1, \ldots, K$, the trend and instantaneous frequencies, respectively, of the signal $f(t)$ in (11) at the time instant t. The signal f in the AHM (11) is said to be *non-stationary* if the phase functions $\phi_k(t)$ are allowed to be non-linear, and it is called a *non-linear signal* if the magnitude functions $A_k(t)$ are allowed to be non-constants. We also introduce the Hilbert spectrum

$$f_{hs}(t) := \sum_{k=1}^{K} A_k(t) e^{i2\pi\phi_k(t)} \tag{12}$$

of f in the AHM (11). Note that this signal f can be written as

$$f(t) = \mathrm{Re}\, f_{hs}(t) + T(t).$$

Hence, after the trend is extracted from f, the Hilbert spectrum (12) facilitates the computation of each signal component f_k of f in (11), as disclosed in detail in our recent paper (Chui and Mhaskar 2015).

The natural approach to find the instantaneous amplitudes (IA's) $A_k(t)$ and instantaneous frequencies (IF's) $\phi_k'(t)$ in (11) is first to decompose the given signal and estimate the IA's and IF's of the signal components separately. It is this approach that we will follow in this paper, to be described in detail in the following section. In this regard, it is important to point out that when the given signal $f \in$ AHM is a blind source, it is definitely not feasible to determine its specific signal components f_k, $k = 1, \ldots, K$, in (11), by any decomposition scheme, without prior knowledge of these components and/or specifying appropriate restrictions on the AHM. Hence, the goal of our paper is not to recover the unknown signal components, but only to modify and improve the *empirical mode decomposition* (EMD) scheme introduced in Huang et al. (1998), allowing real-time implementation and adapting to time-domains of bounded and half-infinite intervals, in order to compute more than one frequency of the signal defined on any time-domain. The interested reader is referred to Daubechies et al. (2011) for the *synchrosqueezed wavelet transform* (SST) approach, and to Chui and Mhaskar (2015) for a direct and local approach, to recover the signal components from a blind source, under certain specifications on the AHM.

This paper is organized as follows. The next section will be devoted to a discussion of the preliminary materials and our hybrid EMD-SST approach. In particular, the EMD scheme, along with its sifting process, via cubic-spline interpolation, is first described, followed by a summary of the SST formulation, together with its real-time algorithm via vanishing-moment (VM) wavelets introduced in Chui et al. (2014). In Sect. 3, our real-time cubic spline local interpolation scheme is constructed, with the

goal of adapting the sifting process to bounded and half-infinite time intervals. The essential properties and computational algorithms of VM wavelets are described in Sect. 4, with numerical examples of our method given in Sect. 5. In Sect. 6, we give the details of the construction, along with proofs, of our local spline interpolation scheme; and in Sect. 7, we compare the results of our hybrid EMD-SST scheme with those of the original EMD approach via the Hilbert transform. In Sect. 8, we end this paper with a brief discussion of replacing EMD by other signal decomposition schemes and of our future investigation by replacing the SST with the direct local approach in Chui and Mhaskar (2015) for our hybrid approach.

2 Preliminaries and discussion of our hybrid approach

This section is divided into three subsections, with the first subsection on a discussion of the sifting process of the EMD scheme, the second subsection on the formulation and description of the SST, and the third subsection on the motivation of our hybrid approach due to the limitations of both the EMD scheme (particularly in adapting the Hilbert transform to bounded and half-infinite intervals) and the SST approach (due to its difficulty in determining the number of signal components and in estimating the instantaneous frequencies based on a single value for the frequency reassignment rule).

2.1 Empirical mode decomposition

The EMD algorithm is one of the first methods to find the IA's $A_k(t)$ and IF's $\phi_k'(t)$ of a given (not necessarily stationary) signal in (11) by first decomposing the signal and then estimating the IA's and IF's of the signal components separately. This is achieved by separating the given signal into a number of oscillating components, called *intrinsic mode functions* (IMF's), and a monotone or slowly oscillating remainder, which may be considered as the trend of the given signal. Each IMF is then extended to its analytic signal extension through the Hilbert transform [as in (1)] in order to compute its IF and IA.

More precisely, given a real-valued signal f, the EMD algorithm starts by setting $h_{1,0} := f$ and computing the cubic spline interpolants of the local maxima and minima of $h_{1,0}$, respectively, called the upper and lower envelopes of h_{10}. Next, it computes the average $m_{1,1}$ of the upper and lower envelopes, and subtracts it from $h_{1,0}$ to obtain $h_{1,1}$. This process of finding upper and lower envelopes and subtracting their mean from the input signal is now repeated on $h_{1,1}$ to find $h_{1,2}, h_{1,3}, h_{1,4}$ and so on, until for some $\ell \geq 1$ the resulting $h_{1,\ell} = h_{1,\ell-1} - m_{1,\ell}$ satisfies the definition of an IMF:

(i) its upper and lower envelopes are (at least approximately) symmetric about the time axis; and
(ii) the difference between its number of local extrema and its number of zero crossings equals -1, 0 or 1.

The first IMF $h_{1,\ell}$ is then denoted by C_1, and this process to find an IMF is called *sifting*. To find the subsequent IMF's C_k, $k = 2, 3, \ldots$, the sifting procedure is repeated on $h_{k,0} := f - C_1 - \cdots - C_{k-1}$. The stopping criterion can be chosen by the user.

The above series of sifting procedures yields a decomposition of the original signal f into K IMF's $C_1, \ldots, C_K$ (for some $K \geq 1$) and a slowly oscillating remainder R_K, written as

$$f(t) = \sum_{k=1}^{K} C_k(t) + R_K(t). \tag{13}$$

This constitutes the first part of the algorithm.

The second part of the algorithm is to find the instantaneous frequency and amplitude of each IMF through Hilbert spectral analysis (HSA), described in (1)–(3), so that

$$\begin{cases} f(t) = \sum_{k=1}^{K} C_k(t) + R_K(t); \\ f_k(t) = B_k(t) \cos 2\pi\theta_k(t), \quad k = 1, \ldots, K, \end{cases} \tag{14}$$

with

$$B_k(t) = |C_k^{\star}(t)|; \qquad \text{and} \qquad \theta_k(t) = \frac{1}{2\pi} \tan^{-1} \frac{(\mathcal{H}C_k)(t)}{C_k(t)}. \tag{15}$$

The derivative $\theta_k'(t)$ of the phase function $\theta_k(t)$ is the IF of the IMF C_k.

However, the EMD scheme, and the current modifications and improvements of it (Wu and Huang 2004, 2009), have several limitations. Firstly, there is no guarantee that the analytic signal extension of an IMF will yield a non-negative IF. This is a serious defect, since negative frequency is meaningless for signals and limits the application of EMD. As discussed in Huang et al. (1998) and Huang and Wu (2008), a necessary condition to obtain a non-negative IF through the Hilbert transform method is a purely oscillatory function with a zero reference level; in fact, this served as the motivation for the definition of an IMF and for EMD to decompose a signal into IMF's. However, this condition is not sufficient to ensure a non-negative IF—indeed, as investigated in Sharpley and Vatchev (2006), there exist several examples of functions that satisfy the definition of an IMF, while its IF calculated through the Hilbert transform method changes sign on intervals of positive measure.

Moreover, since the Hilbert transform is defined for functions $f \in L^p(-\infty, \infty)$ with $p > 1$, while real-life signals are typically defined on bounded or half-infinite intervals, artificial extension of an IMF to the real line is necessary in order to apply the Hilbert transform, often yielding unreliable results.

Another important aspect of EMD is the construction of upper and lower envelopes through interpolation of local maxima and minima. In the original formulation of EMD in Huang et al. (1998), the authors proposed to use standard cubic spline interpolation. Not being a local method, it becomes computationally expensive to obtain the interpolant when the number of extrema becomes very large. Taking care of the boundary values is also somewhat problematic. One solution mentioned in Huang et al. (1998) and Chen et al. (2006) is to extend the data signal at the boundaries according to some user-defined rule; however, this is artificial and does not always yield accurate results.

2.2 Synchrosqueezed wavelet transform

Instead of computing the IF's after the signal is decomposed as is done when applying EMD, the approach that Daubechies et al. (Daubechies et al. 2011; Daubechies and Maes 1996) proposed is first to estimate the IF's of the signal components, under the assumption that the signal satisfies certain strict properties of the AHM in (11), before recovering the signal components of the model. For this purpose, the notion of the synchrosqueezed wavelet transform was introduced to compute a single *reference IF function* through which the IF's of all the signal components are "squeezed out" from the input signal in the form of a digital image, allowing the estimation of the individual IF functions and the signal components themselves.

More precisely, the SST works through "squeezing" the continuous wavelet transform (CWT), defined for any function $g \in L^2(\mathbb{R})$ by the inner product

$$(W_\psi g)(a,b) := \langle g, \psi^{(a,b)} \rangle, \tag{16}$$

with $\psi^{(a,b)}$ given by

$$\psi^{(a,b)}(t) := \frac{1}{a}\psi\left(\frac{t-b}{a}\right), \tag{17}$$

where the analysis wavelet ψ is required to be *admissible* in the sense that its Fourier transform vanishes on the negative frequency axis. The "squeezing out" of IF's is achieved through the single reference IF function

$$\omega_g(a,b) := \begin{cases} \frac{\partial_b (W_\psi g)(a,b)}{2\pi i (W_\psi g)(a,b)}, & \text{if } (W_\psi g)(a,b) \neq 0; \\ -\infty, & \text{otherwise,} \end{cases} \tag{18}$$

called the *frequency reassignment (FRA) rule*. The SST is then computed through

$$(S_{\Gamma,\alpha} f)(b,\xi) = \int_{\{a:|(W_\psi f)(a,b)|>\Gamma\}} (W_\psi f)(a,b) h_\alpha(|\xi - \omega_f(a,b)|) \frac{\mathrm{d}a}{a}, \tag{19}$$

where

$$h_\alpha(x) := \frac{1}{\alpha} h\left(\frac{x}{\alpha}\right), \quad 0 < \alpha << 1 \tag{20}$$

is some "smooth" function so that $\{h_\alpha\}$ converges to the delta distribution for $\alpha \to 0$, and Γ is a thresholding parameter. In other words, the SST is a special type of reassignment method on the CWT which reallocates the values of the CWT from the scale-time point (a,b) to a time–frequency position (b,ξ).

The output of the SST is displayed as a two-dimensional digital image representing a set of "IF curves", which may be extracted through a suitable curve fitting method (Chen et al. 2014; Thakur and Wu 2011). In practice, the curves are extracted one by one, where the image pixels that constitute a particular curve are removed from the image before the next curve is found. This process is repeated until no obvious curve remains in the digital image. The curves extracted in this way are estimations of the IF's $\phi_k'(t)$ of the components constituting the given signal [in (11)]. This curve

extraction process requires supervision, especially if the thresholding parameter is small.

Once the K IF's $\phi_k'(t),\ k = 1, \ldots, K$ have been determined, they may be used to estimate the signal components in the AHM in (11) through

$$f_k^{\Gamma,\Delta}(t) := R_\psi^{-1} \int_{\frac{1-\Delta}{\phi_k'(t)}}^{\frac{1+\Delta}{\phi_k'(t)}} (W_\psi f)(a,t)\chi_{\{a:|(W_\psi f)(a,b)|>\Gamma\}}(a)\frac{\mathrm{d}a}{a},$$

for some sufficiently small constant $\Delta > 0$, with

$$R_\psi := \int_0^\infty \frac{\hat{\psi}(\zeta)}{\zeta}\mathrm{d}\zeta.$$

(This construction formula can be shown to be equivalent to obtaining $f_k^{\Gamma,\Delta}(t)$ through the inverse CWT.)

An obstacle of the SST approach is that the analysis wavelet of the CWT must be admissible so that $\hat{\psi}(\omega) = 0,\ \omega < 0$. Hence, a Meyer-like wavelet was used for the SST in Daubechies et al. (2011) and Daubechies and Maes (1996), with off-line implementation. In our recent work (Chui et al. 2014), the notion of compactly supported spline vanishing moment (VM) wavelets was introduced for real-time computation of the CWT as well as for avoiding numerical estimation of the derivative of the CWT in the FRA rule (18). However, with a single reference IF function ω_g in (18) to estimate the IF's of all the signal components, it is not convincing that the SST approach could yield accurate results, particularly for over 4 or 5 IMF's. Furthermore, since computation of the signal components must depend on the accuracy of the estimated IF's, the SST approach alone cannot be very reliable.

2.3 Our approach

In this paper, we develop a hybrid EMD-SST computational scheme by combining the "best" parts of EMD and SST, as an alternative approach to the original EMD method. In a nutshell, we apply a modified SST to each IMF of the EMD. While our modified SST assures non-negative instantaneous frequencies of the IMF's, the EMD eliminates the guessing work of the number of signal components from the digital image of the original SST approach. More specifically, we modify the SST to process signals on bounded or half-infinite time intervals by applying VM wavelets with stacked knots, and in addition, we replace the Hilbert transform of the original EMD approach by our modified SST to avoid artificial extension of the IMF's to the real line.

Another important contribution of our paper is the formulation of a real-time cubic spline interpolation scheme for a bounded interval for the sifting process of the EMD algorithm. This scheme has a local formulation and is designed to include shape-preserving conditions at the boundary values, which yield more accurate results near the boundaries than the standard cubic spline interpolation used in the original formulation of EMD.

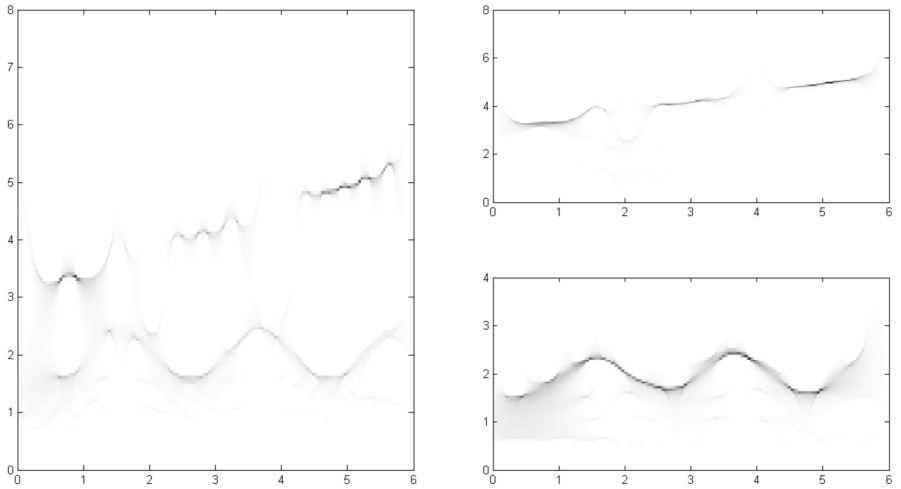

Fig. 1 *Left* the output from the (improved) SST (with our analytic VM wavelet and boundary considerations) applied to the mixed input signal. *Right* the output from the hybrid EMD-SST approach

Lastly, we apply a smoothing spline curve fitting scheme, with automatic optimal smoothing through generalized cross-validation (Wahba 1975; Craven and Wahba 1978; Golub et al. 1979; Carew et al. 2003), to the digital image output of the SST, instead of the custom curve fitting scheme described in Chen et al. (2014).

To illustrate the advantage of first decomposing a given signal using the EMD algorithm before estimating each component's IF using the modified SST, we consider the non-linear, non-stationary signal $f(t) = f_1(t) + f_2(t)$, with

$$f_1(t) = 0.1(t^4 - 12t^3 + 44t^2 - 48t)\cos 2\pi(3t + 0.2t^2);$$
$$f_2(t) = e^{(-0.15t)}\cos 2\pi(2t + 0.2\cos t),$$

so that

$$\phi_1'(t) = 3 + 0.4t \qquad \text{and} \qquad \phi_2'(t) = 2 - 0.2\sin t.$$

In Fig. 1, we display the result of the original SST approach applied to the mixed signal, where we used our analytic VM wavelet in the CWT with boundary considerations, as well as the result of our hybrid EMD-SST approach. We note that, as a result of first applying EMD to separate the input signal into IMF components, the shapes of the IF curves displayed in the digital SST images from our hybrid EMD-SST approach are much clearer than in the original SST output.

3 Construction of envelopes through blending

In this section, we introduce the completely local interpolation scheme to be used in the sifting process of EMD to construct upper and lower envelopes (through interpolation of the local maxima and minima, respectively).

For a given sequence

$$\mathbf{x} : x_{-3} = \cdots = a = x_0 < x_1 < \cdots < x_{N+1} = b = \cdots = x_{N+4},$$

let $S_{\mathbf{x},4}[a, b]$ denote the linear space of cubic polynomial splines on $[a, b]$ with knots in $\mathbf{x}$. The set of normalized cubic B-splines

$$\left\{N_{\mathbf{x},4,j} : \ j = -3, \ldots, N\right\}$$

is a locally supported basis for $S_{\mathbf{x},4}[a, b]$ (Curry and Schoenberg 1966). The cubic B-splines $N_{\mathbf{x},4,j}$ are defined in terms of divided differences of truncated powers by

$$N_{\mathbf{x},4,j}(x) := (x_{j+4} - x_j)[x_j, \ldots, x_{j+4}](\cdot - x)_+^3, \quad j = -3, \ldots, N, \tag{21}$$

where the divided differences are defined by

$$[u, \ldots, u]g := \frac{g^\ell(u)}{\ell!} \tag{22}$$

if there are $\ell + 1$ entries in $[u \ldots, u]$, and

$$[u_0, \ldots, u_n]g := \frac{[u_1, \ldots, u_n]g - [u_0, \ldots, u_{n-1}]g}{u_n - u_0} \tag{23}$$

if $u_0 \le u_1 \le \cdots \le u_n$ with $u_n > u_0$, where $[u_i]g := g(u_i)$. Truncated powers are defined by

$$x_+^n := (\max\{0, x\})^n. \tag{24}$$

Given a signal f, our objective is to construct an interpolation operator $\mathcal{P}$ in terms of the cubic B-splines in (21) such that the following conditions are satisfied:

(i) $\mathcal{P}$ is local in the sense that the value of $\mathcal{P}f$ at any $x^* \in [x_i, x_{i+1}]$ inside $[a, b]$ only depends on the values of f in the neighborhood $[x_{i-6}, x_{i+7}]$ of x^*;

(ii) $\mathcal{P}$ preserves polynomials of degree $n \le 3$; that is,

$$(\mathcal{P}p)(x) = p(x), \quad p \in \pi_3, \ x \in [a, b]; \tag{25}$$

(iii) $\mathcal{P}f$ interpolates f at the values $x_0, \ldots, x_{N+1}$; that is,

$$(\mathcal{P}f)(x_i) = f(x_i), \ i = 0, 1, \ldots, N + 1; \tag{26}$$

(iv) $\mathcal{P}$ preserves derivatives of f at x_0 and x_{N+1} with

$$\begin{cases} (\mathcal{P}f)^{(n)}(x_0) = f^{(n)}(x_0), & n = 1, 2, 3; \\ (\mathcal{P}f)^{(n)}(x_{N+1}) = f^{(n)}(x_{N+1}), & n = 1, 2. \end{cases} \tag{27}$$

In (iv), since the derivatives of a signal f are generally not known in practice, we approximate the nth derivative of f at x_0 and x_{N+1} by the nth order divided difference of f at x_0 and x_{N+1}, respectively, when applying our method.

Our idea is to develop a locally supported quasi-interpolation operator $\mathcal{Q}$ (as introduced by de Boor and Fix 1973) in terms of the cubic B-splines on the bounded interval $[a, b]$ to achieve properties (i) and (ii). Our quasi-interpolation method is based on a quasi-interpolation scheme for real-time application described in Chen et al. (1988). We remark that the method in Chen et al. (1988) is derived for data values on an unbounded interval, and it is adapted here for the bounded interval $[a, b]$.

Then, to achieve the interpolation conditions (iii) and (iv) above (while preserving local support), we will develop a local interpolation operator $\mathcal{R}$ as well, which, together with the quasi-interpolation operator $\mathcal{Q}$, leads to the *blending operator* $\mathcal{P}$, introduced in Chui and Diamond (1990), defined by

$$\mathcal{P} := \mathcal{R} \oplus \mathcal{Q}, \tag{28}$$

where

$$\mathcal{R} \oplus \mathcal{Q} := \mathcal{Q} + \mathcal{R}(\mathcal{I} - \mathcal{Q}) = \mathcal{Q} + \mathcal{R} - \mathcal{R}\mathcal{Q}, \tag{29}$$

with $\mathcal{I}$ denoting the identity operator. From this formulation, it becomes clear that the idea of the blending operation is to first apply the local quasi-interpolation operator $\mathcal{Q}$ to f to ensure high approximation order and smoothness, and then to apply the local interpolation operator $\mathcal{R}$ to the error produced by $\mathcal{Q}$ to achieve interpolation at the interpolation points $x_0, \ldots, x_{N+1}$ and preservation of the derivatives at the boundaries $x = a$ and $x = b$. (Note that the operators $\mathcal{Q}$ and $\mathcal{R}$ are not commutative.)

This interpolation scheme may be applied in the context of constructing upper and lower envelopes during the sifting procedure of EMD, with the interpolation points x_i equal to the local maxima and minima, respectively. For easy implementation, we note that the knot sequence $\mathbf{x}$ for the cubic B-splines (which form the basis functions of our interpolation scheme) is chosen to coincide with the interpolation points $x_0, \ldots, x_{N+1}$ (with the stacked knots $x_{-3} = x_{-2} = x_{-1} = x_0$ and $x_{N+1} = x_{N+2} = x_{N+3} = x_{N+4}$ appended on either side).

We proceed, in Sects. 3.1–3.3, to describe the quasi-interpolation operator $\mathcal{Q}$, the local interpolation operator $\mathcal{R}$, and the blending operator $\mathcal{P}$, respectively.

3.1 Quasi-interpolation operator

To define the quasi-interpolation operator $\mathcal{Q}$, we will need the following notations.

First, $D(x_k, \ldots, x_{k+\ell})$ denotes the Vandermonde determinant of $x_k, \ldots, x_{k+\ell}$; that is,

$$D(x_k, \ldots, x_{k+\ell}) = \begin{vmatrix} 1 & 1 & \cdots & 1 \\ x_k & x_{k+1} & \cdots & x_{k+\ell} \\ \vdots & \vdots & & \vdots \\ x_k^\ell & x_{k+1}^\ell & \cdots & x_{k+\ell}^\ell \end{vmatrix}; \tag{30}$$

and $D(x_k, \ldots, x_{k+q-1}, \xi_j, x_{k+q+1}, \ldots, x_{k+\ell})$ is obtained from $D(x_k, \ldots, x_{k+\ell})$ by replacing its qth column with the vector

$$\xi_j := [\xi^0(j), \ldots, \xi^\ell(j)]^T, \tag{31}$$

with

$$\begin{cases} \xi^0(j) = 1; \\ \xi^n(j) = \frac{\sigma^n(x_{j+1}, \ldots, x_{j+\ell})}{\binom{\ell}{n}}, \quad n = 1, \ldots, \ell; \end{cases} \tag{32}$$

and where $\sigma^n(r_1, \ldots, r_s)$ denotes the classical symmetric function, defined by

$$\begin{cases} \sigma^0(r_1, \ldots, r_s) = 1; \\ \sigma^n(r_1, \ldots, r_s) = \displaystyle\sum_{1 \le t_1 < t_2 < \cdots < t_n \le s} r_{t_1} r_{t_2} \cdots r_{t_n}, \quad n = 1, \ldots, \ell. \end{cases} \tag{33}$$

Furthermore, $D_C(x_k, \ldots, x_{k+n}, x_{k+n}^{(1)}, \ldots, x_{k+n}^{(p)}, x_{k+n+1}, \ldots, x_{k+\ell})$ denotes the confluent Vandermonde determinant; that is, for $j = 1, \ldots, p$, the $(n+1+j)$th column of D_C is given by

$$(D_C)_{i,n+1+j} = \begin{cases} 0 & \text{if } i \le j; \\ \frac{(i-1)!}{(i-1-j)!} x_{k+n}^{i-1-j} & \text{if } i > j. \end{cases}$$

(In other words, confluent columns are derivatives of the original Vandermonde columns.) The remaining $\ell + 1$ columns of D_C are regular Vandermonde columns corresponding to $x_k, \ldots, x_{k+\ell}$ [as in (30)]. Similar as above, $D_C(x_k, \ldots, x_{k+n}, x_{k+n}^{(1)}, \ldots, x_{k+n}^{(q-1)}, \xi_j, x_{k+n}^{(q+1)}, \ldots, x_{k+n}^{(p)}, x_{k+n+1}, \ldots, x_{k+\ell})$ is obtained from $D_C(x_k, \ldots, x_{k+n}, x_{k+n}^{(1)}, \ldots, x_{k+n}^{(p)}, x_{k+n+1}, \ldots, x_{k+\ell})$ by replacing its $(n+q+1)$th column with ξ_j.

Definition 1 (*Quasi-interpolation operator*) The quasi-interpolation operator $\mathcal{Q}$ is defined by

$$(\mathcal{Q}f)(x) := \sum_{\ell=1}^{3} f^{(\ell)}(x_0) M_{-\ell}(x) + \sum_{i=0}^{N+1} f(x_i) M_i(x) + \sum_{r=1}^{2} f^{(r)}(x_{N+1}) M_{N+1+r}(x), \tag{34}$$

in terms of the *spline molecules*

$$\begin{cases} M_{-\ell}(x) := \displaystyle\sum_{j=0}^{3-\ell} a_{-\ell,j} N_{\mathbf{x},4,j-3}(x), \quad \ell = 1, 2, 3; \\ M_i(x) := \displaystyle\sum_{j=0}^{3} a_{i,j} N_{\mathbf{x},4,i+j-3}(x), \quad i = 0, \ldots, N; \\ M_{N+1+r}(x) := \displaystyle\sum_{j=r}^{2} a_{N+1+r,j} N_{\mathbf{x},4,N+j-2}(x), \quad r = 0, 1, 2, \end{cases} \tag{35}$$

where the coefficients are given by:

– For $i = 0, 1, 2,\ j = 3 - i, \ldots, 3$ and $i = 3, \ldots, N - 3,\ j = 0, \ldots, 3$ and $i = N - 2, \ldots, N,\ j = 0, \ldots, N - i$:

$$a_{i,j} = \frac{D(x_{i+j-3}, \ldots, x_{i-1}, \xi_{i+j-3}, x_{i+1}, \ldots, x_{i+j})}{D(x_{i+j-3}, \ldots, x_{i+j})}; \tag{36}$$

– For $i = 0, 1, 2,\ j = 0, \ldots, 2 - i$:

$$a_{i,j} = \frac{D_C(x_0, \ldots, x_0^{(3-i-j)}, x_1, \ldots, x_{i-1}, \xi_{i+j-3}, x_{i+1}, \ldots, x_{i+j})}{D_C(x_0, \ldots, x_0^{(3-i-j)}, x_1, \ldots, x_{i+j})}; \tag{37}$$

– For $\ell = 1, 2, 3,\ j = 0, \ldots, 3 - \ell$:

$$a_{-\ell,j} = \frac{D_C(x_0, \ldots, x_0^{(\ell-1)}, \xi_{j-3}, x_0^{(\ell+1)}, \ldots, x_0^{(3-j)}, x_1, \ldots, x_j)}{D_C(x_0, \ldots, x_0^{(3-j)}, x_1, \ldots, x_j)}; \tag{38}$$

– For $i = N - 2, \ldots, N,\ j = N - i + 1, \ldots, 3$:

$$a_{i,j} = \frac{D_C(x_{i+j-3}, \ldots, x_{i-1}, \xi_{i+j-3}, x_{i+1}, \ldots, x_{N+1}, x_{N+1}^{(1)}, \ldots, x_{N+1}^{(i+j-N-1)})}{D_C(x_{i+j-3}, \ldots, x_{N+1}, x_{N+1}^{(1)}, \ldots, x_{N+1}^{(i+j-N-1)})}; \tag{39}$$

– For $r = 0, 1, 2,\ j = r, \ldots, 2$:

$$a_{N+1+r,j} = \frac{D_C(x_{N+j-2}, \ldots, x_{N+1}, x_{N+1}^{(1)}, \ldots, x_{N+1}^{(r-1)}, \xi_{N+j-2}, x_{N+1}^{(r+1)}, \ldots, x_{N+1}^{(j)})}{D_C(x_{N+j-2}, \ldots, x_{N+1}, x_{N+1}^{(1)}, \ldots, x_{N+1}^{(j)})}. \tag{40}$$

We note that the molecules in the definition above are compactly supported, with

$$\begin{cases} \text{supp} M_{-\ell} = [x_0, x_{4-\ell}], & \ell = 1, 2, 3; \\ \text{supp} M_i = [x_{i-3}, x_{i+4}], & i = 0, \ldots, N; \\ \text{supp} M_{N+1+r} = [x_{N-2+r}, x_{N+1}], & r = 0, 1, 2. \end{cases} \tag{41}$$

With these definitions, we can show that (25) in condition (ii) above is satisfied.

Theorem 1 *For $N \geq 9$, the quasi-interpolation operator $\mathcal{Q}$, formulated in (34) in Definition 1, satisfies the condition*

$$(\mathcal{Q}p)(x) = p(x) \tag{42}$$

for all $x \in [a, b]$ and $p \in \pi_3$.

We leave the proof until Sect. 6.

3.2 Local interpolation operator

Next, we define the local interpolation operator $\mathcal{R}$ to achieve properties (iii) and (iv) above, while preserving local support. To construct $\mathcal{R}$, we will consider a knot sequence $\tilde{\mathbf{x}} \supset \mathbf{x}$, constructed by inserting one additional knot in between every two (unstacked) knots of $\mathbf{x}$, so that

$$\tilde{x}_{2j+2} = x_j, \quad j = 1, \ldots, N.$$

Furthermore, to facilitate the Hermite interpolation conditions (27) at the boundaries $x = x_0$ and $x = x_{N+1}$, we will insert three evenly spaced additional knots $\tilde{x}_1, \tilde{x}_2, \tilde{x}_3$ in the interval (x_0, x_1), with $\tilde{x}_0 := x_0$, as well as two evenly spaced additional knots $\tilde{x}_{2N+3}, \tilde{x}_{2N+4}$ in the interval (x_N, x_{N+1}), with $\tilde{x}_{2N+5} := x_{N+1}$. Also, the knot sequence $\tilde{\mathbf{x}}$ is extended with stacked knots in the same way as $\mathbf{x}$, so that $\tilde{x}_i = x_i,\ i = -1, -2, -3$ and $\tilde{x}_{2j+5+i} = x_{N+1+i},\ i = 1, 2, 3$.

In the following, we will use the notation $N_{\{\tilde{x}_a, \tilde{x}_b, \tilde{x}_c, \tilde{x}_d, \tilde{x}_e\}, 4}$ to denote the cubic B-spline spanning the knots $\{\tilde{x}_a, \tilde{x}_b, \tilde{x}_c, \tilde{x}_d, \tilde{x}_e\}$. We will make use of the particular sequences

$$\begin{cases} \tilde{\mathbf{x}}_{-3} = \{\tilde{x}_{-3}, \ldots, \tilde{x}_0, \tilde{x}_4\}; & \tilde{\mathbf{x}}_1 = \{\tilde{x}_1, \tilde{x}_2, \tilde{x}_4, \tilde{x}_5, \tilde{x}_6\}; \\ \tilde{\mathbf{x}}_{-2} = \{\tilde{x}_{-2}, \ldots, \tilde{x}_0, \tilde{x}_2, \tilde{x}_4\}; & \tilde{\mathbf{x}}_{N+1} = \{\tilde{x}_{2N+2}, \ldots, \tilde{x}_{2N+6}\}; \\ \tilde{\mathbf{x}}_{-1} = \{\tilde{x}_{-1}, \tilde{x}_0, \tilde{x}_1, \tilde{x}_2, \tilde{x}_4\}; & \tilde{\mathbf{x}}_{N+2} = \{\tilde{x}_{2N+2}, \tilde{x}_{2N+3}, \tilde{x}_{2N+5}, \ldots, \tilde{x}_{2N+7}\}; \\ \tilde{\mathbf{x}}_0 = \{\tilde{x}_0, \ldots, \tilde{x}_4\}; & \tilde{\mathbf{x}}_{N+3} = \{\tilde{x}_{2N+2}, \tilde{x}_{2N+5}, \ldots, \tilde{x}_{2N+8}\}. \end{cases}$$

Definition 2 (*Local interpolation operator*) The local interpolation operator $\mathcal{R}$ is defined by

$$(\mathcal{R}f)(x) := \sum_{\ell=1}^{3} f^{(\ell)}(x_0) L_{-\ell}(x) + \sum_{i=0}^{N+1} f(x_i) L_i(x) + \sum_{r=1}^{2} f^{(r)}(x_{N+1}) L_{N+1+r}(x), \tag{43}$$

in terms of the spline molecules

$$\begin{cases} L_{-\ell}(x) := \sum_{k=0}^{3} b_{-\ell,k} N_{\tilde{\mathbf{x}}_{-3+k}, 4}(x), \quad \ell = 0, 1, 2, 3; \\ L_1(x) := \frac{N_{\tilde{\mathbf{x}}_1, 4}(x)}{N_{\tilde{\mathbf{x}}_1, 4}(x_1)}; \\ L_i(x) := \frac{N_{\tilde{\mathbf{x}}, 4, 2i}(x)}{N_{\tilde{\mathbf{x}}, 4, 2i}(x_i)}, \quad i = 2, \ldots, N; \\ L_{N+1+r}(x) := \sum_{k=0}^{2} b_{N+1+r,k} N_{\tilde{\mathbf{x}}_{N+1+k}, 4}(x), \quad r = 0, 1, 2, \end{cases} \tag{44}$$

with the coefficients $b_{-\ell,k},\ k, \ell = 0, 1, 2, 3$ and $b_{N+1+r,k},\ k, r = 0, 1, 2$ determined by the conditions

$$L_{-\ell}^{(n)}(x_0) = \delta_{\ell-n},\ \ell, n = 0, 1, 2, 3; \quad L_{N+1+r}^{(n)}(x_{N+1}) = \delta_{r-n},\ r, n = 0, 1, 2, \tag{45}$$

where δ_{i-j} denotes the Kronecker delta function

$$\delta_{i-j} := \begin{cases} 1 & \text{if } i = j; \\ 0 & \text{otherwise.} \end{cases}$$

The above molecules are compactly supported, with

$$\begin{cases} \text{supp} L_{-\ell} = [x_0, x_1], \quad \ell = 0, 1, 2, 3; \\ \text{supp} L_1 = [\tilde{x}_1, x_2]; \\ \text{supp} L_i = [x_{i-1}, x_{i+1}], \quad i = 2, \ldots, N; \\ \text{supp} L_{N+1+r} = [x_N, x_{N+1}], \quad r = 0, 1, 2. \end{cases} \tag{46}$$

From the construction in (44), it is clear that

$$L_i(x_j) = \delta_{i-j}, \quad i = 1, \ldots, N; \ j = 0, \ldots, N+1. \tag{47}$$

By using also (45), the following result follows immediately.

Theorem 2 *The local interpolation operator $\mathcal{R}$, formulated in* (43) *in Definition 2, satisfies the Hermite interpolation conditions*

$$(\mathcal{R}f)(x_i) = f(x_i), \quad i = 0, \ldots, N+1,$$

and

$$\begin{cases} (\mathcal{R}f)^{(n)}(x_0) = f^{(n)}(x_0), \quad n = 1, 2, 3; \\ (\mathcal{R}f)^{(n)}(x_{N+1}) = f^{(n)}(x_{N+1}), \quad n = 1, 2. \end{cases}$$

3.3 Blending operator

With $\mathcal{Q}$ and $\mathcal{R}$ formulated in Definitions 1 and 2, respectively, the blending operator $\mathcal{P}$ is now given by (28), (29).

An equivalent formulation of $\mathcal{P}$ may be obtained by expanding (29) in terms of the spline molecules M_i and L_i, $i = -3, \ldots, N+3$, so that $\mathcal{P}$ is given by

$$(\mathcal{P}f)(x) = \sum_{\ell=1}^{3} f^{(\ell)}(x_0) J_{-\ell}(x) + \sum_{i=0}^{N+1} f(x_i) J_i(x) + \sum_{r=1}^{2} f^{(r)}(x_{N+1}) J_{N+1+r}(x), \tag{48}$$

in terms of the spline *i-molecules* J_i, given by

$$\begin{cases} J_{-\ell}(x) = M_{-\ell}(x) + L_{-\ell}(x) - \sum_{j=0}^{3-\ell} M_{-\ell}(x_j)L_j(x) - \sum_{k=1}^{3} M_{-\ell}^{(k)}(x_0)L_{-k}(x), \\ \qquad\qquad\qquad\qquad\qquad\qquad\qquad\qquad \ell = 1, 2, 3; \\ J_i(x) = M_i(x) + L_i(x) - \sum_{j=i-3}^{i+4} M_i(x_j)L_j(x) - \sum_{k=1}^{3} M_i^{(k)}(x_0)L_{-k}(x) \\ \qquad\qquad - \sum_{n=1}^{2} M_i^{(n)}(x_{N+1})L_{N+1+n}(x), \quad i = 0, \ldots, N+1; \\ J_{N+1+r}(x) = M_{N+1+r}(x) + L_{N+1+r}(x) - \sum_{j=N-2+r}^{N} M_{N+1+r}(x_j)L_j(x) \\ \qquad\qquad - \sum_{k=1}^{2} M_{N+1+r}^{(k)}(x_{N+1})L_{N+1+k}(x), \quad r = 1, 2. \end{cases} \tag{49}$$

We can show that $\mathcal{P}$ then achieves all four conditions (i)–(iv).

Theorem 3 *The blending operator $\mathcal{P}$, defined by (28), (29), is local and satisfies the polynomial preservation property of the quasi-interpolation operator $\mathcal{Q}$ as well as the Hermite interpolation conditions of the local interpolation operator $\mathcal{R}$; that is, $\mathcal{P}$ satisfies (25), (26) and (27).*

We leave the proof until Sect. 6.

4 VM wavelets

We now describe the analytic vanishing moment (VM) wavelets, introduced in Chui et al. (2014), to be applied as the analysis wavelet in the CWT as part of the SST.

For an integer $m \geq 1$ and an arbitrary knot sequence $\mathbf{x}$ with $x_{j+1} \geq x_j$ and $x_{j+m} > x_j$ for all $j \in \mathbb{Z}$, the normalized mth order B-splines $N_{\mathbf{x},m,j}$ are defined by

$$N_{\mathbf{x},m,j}(x) := (x_{j+m} - x_j)[x_j, \ldots, x_{j+m}](\cdot - x)_+^{m-1}, \quad j \in \mathbb{Z} \tag{50}$$

[the general case of (21)], with the divided differences and truncated powers defined in (22)–(24). Then, for an integer $n \geq 1$, the vanishing moment wavelets $\psi_{\mathbf{x},m,n,j}$, $j \in \mathbb{Z}$, are constructed in Chui et al. (2014) in terms of the mth order B-splines to have minimum support and satisfy the n vanishing moment conditions

$$\begin{cases} \int_{-\infty}^{\infty} x^{\ell} \psi_{\mathbf{x},m,n,j}(x)\mathrm{d}x = 0, \quad \ell = 0, 1, \ldots, n-1; \\ \int_{-\infty}^{\infty} x^{n} \psi_{\mathbf{x},m,n,j}(x)\mathrm{d}x \neq 0. \end{cases}$$

Under these conditions, it is shown in (Chui et al., 2014, Theorem 3.2) that the VM wavelets $\psi_{\mathbf{x},m,n,j}$ satisfy the unique formulation (up to a non-zero constant multiple)

$$\psi_{\mathbf{x},m,n,j}(x) = N_{\mathbf{x},m+n,j}^{(n)}(x), \quad j \in \mathbb{Z}. \tag{51}$$

An immediate consequence of (51) is that the derivative of a VM wavelet is also a VM wavelet, with

$$\psi'_{\mathbf{x},m,n,j}(x) = \psi_{\mathbf{x},m-1,n+1,j}(x), \quad j \in \mathbb{Z}$$

(Chui et al., 2014, Corollary 3.3).

For our application of the VM wavelets as analysis wavelets in the CWT, let us consider the knot sequence

$$\mathbf{x} : x_{-m+1} = \cdots = -L = x_0 < x_1 < \cdots < x_{m+n} = L = \cdots = x_{2m+n-1}, \tag{52}$$

with $x_0, \ldots, x_{m+n}$ uniformly spaced in the bounded interval $[-L, L]$, so that

$$x_j = -L + jh, \ j = 0, \ldots, m+n, \tag{53}$$

with knot spacing

$$h := \frac{2L}{(m+n)}. \tag{54}$$

In this setting, we may derive a representation for the *interior wavelet* $\psi_{\mathbf{x},m,n,0}$ in terms of the normalized mth order B-splines from (51) by applying the formula (de Boor 2001, p. 131)

$$N'_{\mathbf{x},\ell,k}(x) = \frac{\ell - 1}{x_{\ell+k-1} - x_k} N_{\mathbf{x},\ell-1,k}(x) - \frac{\ell - 1}{x_{\ell+k} - x_{k+1}} N_{\mathbf{x},\ell-1,k+1}(x) \tag{55}$$

n times, starting with $N^{(n)}_{\mathbf{x},m+n,0}$, which leads to the formula

$$\psi_{\mathbf{x},m,n,0}(x) = \frac{1}{h^n} \sum_{k=0}^{n} (-1)^k \binom{n}{k} N_{\mathbf{x},m,0}(x - kh).$$

We note that the support of $\psi_{\mathbf{x},m,n,0}$ spans the entire interval, so that

$$\text{supp}\psi_{\mathbf{x},m,n,0} = [-L, L].$$

The $m-1$ *boundary wavelets* $\psi_{\mathbf{x},m,n,j}$, $j = -m+1, \ldots, -1$ at the left hand side endpoint $x = -L$, with supports

$$\text{supp}\psi_{\mathbf{x},m,n,j} = [-L, L + jh], \quad j = -m+1, \ldots, -1,$$

and the $m-1$ boundary wavelets $\psi_{\mathbf{x},m,n,j}$, $j = 1, \ldots, m-1$ at the right hand side endpoint $x = L$, with supports

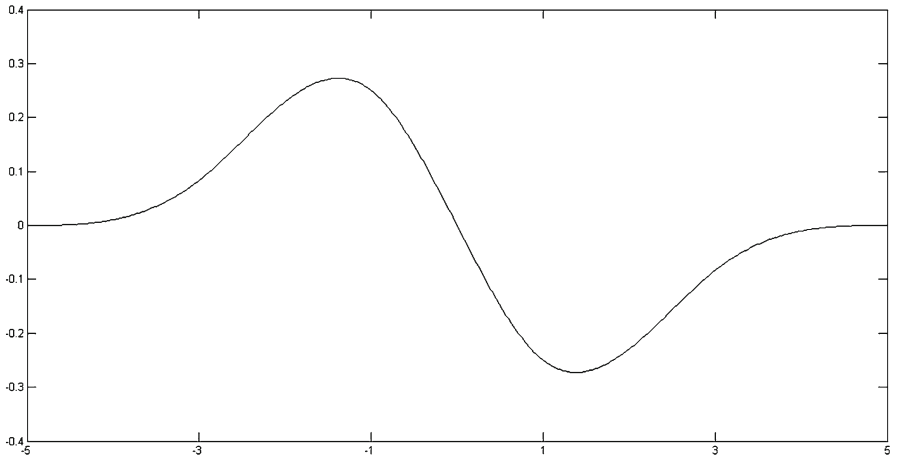

Fig. 2 Interior wavelet $\psi_{\mathbf{x},4,1,0}$ on the interval $[-5, 5]$

$$\text{supp}\psi_{\mathbf{x},m,n,j} = [-L + jh, L], \quad j = 1, \ldots, m-1,$$

may be obtained similarly by applying (55) n times to (51), starting with $N^{(n)}_{\mathbf{x},m+n,j}$ for $j = -m+1, \ldots, -1,\ 1, \ldots, m-1$, respectively.

Specifically, for $m = 4$ and $n = 1$, we have the following.

Theorem 4 *For the knot sequence* $\mathbf{x}$ *in* (52), (53), (54) *with* $m = 4$ *and* $n = 1$, *the cubic VM wavelets with 1 vanishing moment are given by*

$$\begin{cases} \psi_{\mathbf{x},4,1,0}(x) = \frac{1}{h}\left(N_{\mathbf{x},4,0}(x) - N_{\mathbf{x},4,0}(x-h)\right); \\ \psi_{\mathbf{x},4,1,j}(x) = \frac{4}{h}\left(\frac{1}{4+j}N_{\mathbf{x},4,j}(x) - \frac{1}{5+j}N_{\mathbf{x},4,j+1}(x)\right), \quad j = -3, -2, -1; \\ \psi_{\mathbf{x},4,1,j}(x) = \frac{4}{h}\left(\frac{1}{5-j}N_{\mathbf{x},4,j}(x) - \frac{1}{4-j}N_{\mathbf{x},4,j+1}(x)\right), \quad j = 1, 2, 3. \end{cases} \tag{56}$$

The derivatives of the VM wavelets $\psi_{\mathbf{x},4,1,j}$, $j = -3, \ldots, 3$ *are given by*

$$\psi'_{\mathbf{x},4,1,j}(x) = \psi_{\mathbf{x},3,2,j}(x), \quad j = -3, \ldots, 3.$$

The cubic VM wavelets in Theorem 4 are shown in Figs. 2 and 3 (with the specific choice of $L = 5$).

The VM wavelets $\psi_{\mathbf{x},3,2,j}$, $j = -3, \ldots, 3$, can be obtained similarly to $\psi_{\mathbf{x},4,1,j}$, $j = -3, \ldots, 3$, in (56) by applying the formula (55) twice to (51) (with $m = 3$ and $n = 2$). This leads to the formulations in terms of quadratic B-splines (defined in (50) with $m = 3$)

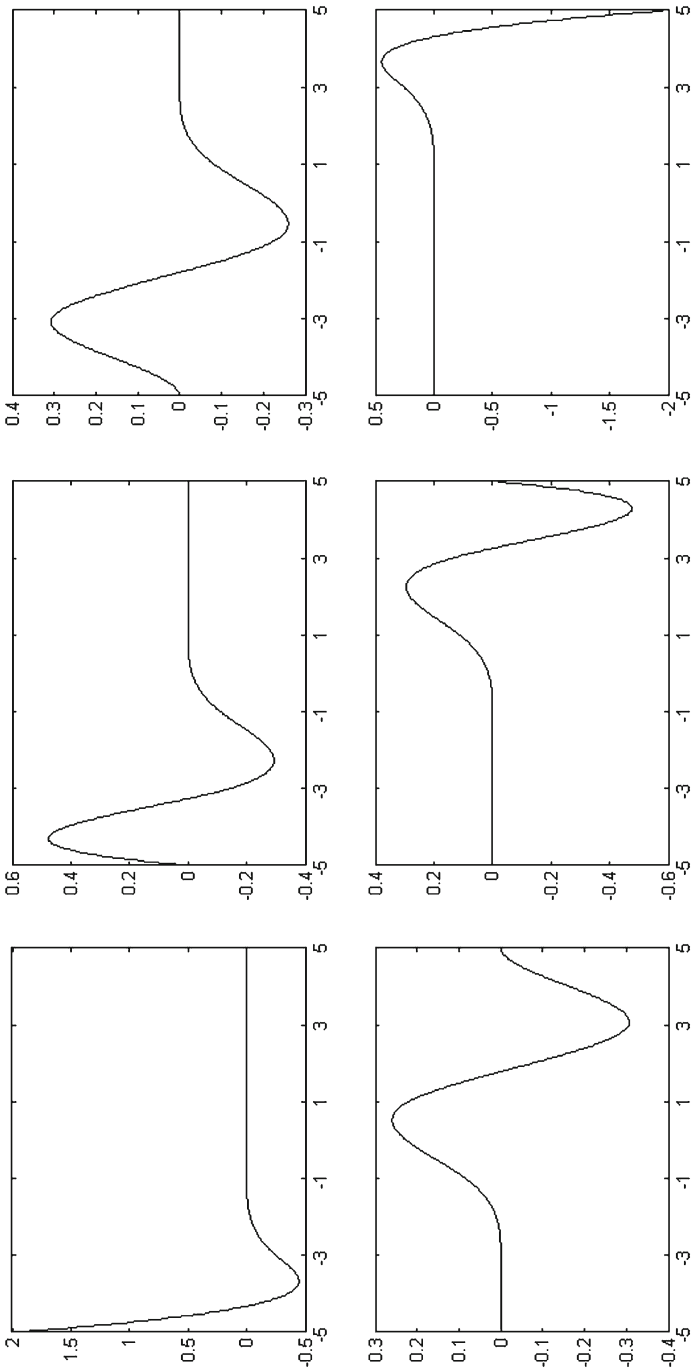

Fig. 3 Boundary wavelets on the interval $[-5, 5]$. *Top, left to right:* $\psi_{\mathbf{x},4,1,-3}$, $\psi_{\mathbf{x},4,1,-2}$ and $\psi_{\mathbf{x},4,1,-1}$. *Bottom, left to right:* $\psi_{\mathbf{x},4,1,1}$, $\psi_{\mathbf{x},4,1,2}$ and $\psi_{\mathbf{x},4,1,3}$

$$\begin{cases} \psi_{\mathbf{x},3,2,0}(x) = \frac{1}{h^2}\left(N_{\mathbf{x},3,0}(x) - 2N_{\mathbf{x},3,0}(x-h) + N_{\mathbf{x},3,0}(x-2h)\right); \\ \psi_{\mathbf{x},3,2,-3}(x) = \frac{12}{h}\left(-\frac{3}{2}N_{\mathbf{x},3,-2}(x) + \frac{1}{4}N_{\mathbf{x},3,-1}(x)\right); \\ \psi_{\mathbf{x},3,2,j}(x) = \frac{12}{h}\left(\frac{1}{(4+j)(3+j)}N_{\mathbf{x},3,j}(x) - \left[\frac{1}{(4+j)^2} + \frac{1}{(5+j)(4+j)}\right]N_{\mathbf{x},3,j+1}(x)\right. \\ \qquad\qquad \left. + \frac{1}{3(5+j)}N_{\mathbf{x},3,j+2}(x)\right), \quad j = -2, -1; \\ \psi_{\mathbf{x},3,2,j}(x) = \frac{12}{h}\left(\frac{1}{3(5-j)}N_{\mathbf{x},3,j}(x) - \left[\frac{1}{(4+j)^2} + \frac{1}{(5+j)(4+j)}\right]N_{\mathbf{x},3,j+1}(x)\right. \\ \qquad\qquad \left. + \frac{1}{(4-j)(3-j)}N_{\mathbf{x},3,j+2}(x)\right), \quad j = 1, 2; \\ \psi_{\mathbf{x},3,2,3}(x) = \frac{12}{h}\left(\frac{1}{4}N_{\mathbf{x},3,3}(x) - \frac{3}{2}N_{\mathbf{x},3,4}(x)\right). \end{cases} \tag{57}$$

We now turn our attention to applying the VM wavelets $\psi_{\mathbf{x},4,1,j},\ j = -3, \ldots, 3$, developed in this section to the CWT, defined in (16), employed as part of the SST, defined in (18), (19) and (20).

To this end, our first task is to pick an analysis wavelet ψ that is admissible according to the definition of the frequency reassignment rule in (18); that is, it satisfies the property $\hat{\psi}(\omega) = 0,\ \omega < 0$. With the definition

$$\psi_j(x) := \psi_{\mathbf{x},4,1,j}(x), \quad j = -3, \ldots, 3,$$

we will consider the analytic representation of ψ_j, given by

$$\psi_j^\star(x) = \psi_j(x) + i(\mathcal{H}\psi_j)(x), \tag{58}$$

called *analytic VM wavelets*. We note that $\psi_j^\star$ is admissible, since

$$\begin{aligned} \hat{\psi}_j^\star(\omega) = \hat{\psi}_j(\omega) + i\widehat{(\mathcal{H}\psi_j)}(\omega) &= \hat{\psi}_j(\omega) + i(-i\,\mathrm{sgn}\,\omega)\hat{\psi}_j(\omega) \\ &= \begin{cases} 2\hat{\psi}_j(\omega) & \text{if } \omega \geq 0; \\ 0 & \text{if } \omega < 0. \end{cases} \end{aligned}$$

We therefore use $\psi_0^\star$ as the "center" interior analysis wavelet in the CWT, while $\psi_j^\star,\ j = -3, \ldots, -1, 1, \ldots, 3$, are used to take care of the boundaries at $x = -L$ and $x = L$, respectively. The scaling and translation operations indicated in (17) are applied as follows:

When scaling by $0 < a < 1$, $\psi_0(\frac{x}{a})$ is a VM wavelet on the uniformly spaced knot sequence

$$\mathbf{x}_a : -L < -L + ah < -L + 2ah < \cdots < L - 2ah < L - ah < L,$$

with knot spacing ah, where $h := \frac{2L}{5}$, according to (54), and with the support of $\psi_0(\frac{x}{a})$ given by

$$\mathrm{supp}\psi_0(\tfrac{x}{a}) = [-aL, aL].$$

$\psi_0(\frac{x}{a})$ is also translated by $\frac{b}{a}$, where $-L(1-a) \leq b \leq L(1-a)$, to ensure that $\psi_0(\frac{x-b}{a})$ stays inside the bounded interval $[-L, L]$.

For the boundary wavelets, we scale by $0 < a < 1$ and let $b = -L(1-a)$, so that the supports of $\psi_j(\frac{x-b}{a})$, $j = -3, -2, -1$ are given by

$$\text{supp}\psi_j(\tfrac{x-b}{a}) = [-L, -L(1-2a) + jah], \quad j = -3, -2, -1;$$

while for $b = L(1-a)$, the supports of $\psi_j(\frac{x-b}{a})$, $j = 1, 2, 3$ are given by

$$\text{supp}\psi_j(\tfrac{x-b}{a}) = [L(1-2a) + jah, L], \quad j = 1, 2, 3.$$

As mentioned earlier, the derivative property in Theorem 4 is one of the key reasons for employing the VM wavelets in the SST. The first step in the execution of the SST is to calculate the FRA rule in (18), and this involves the calculation of the derivative of the CWT. From Theorem 4, we have an explicit formulation for this derivative—therefore, the FRA rule in (18) applied to a function g becomes

$$(\omega_g)(a,b) = \frac{\partial_b(W_{\psi_j^\star}g)(a,b)}{2\pi i(W_{\psi_j^\star}g)(a,b)} = \frac{\langle g(x), \partial_b\psi_j^\star(\frac{x-b}{a})\rangle}{2\pi i\langle g(x), \psi_j^\star(\frac{x-b}{a})\rangle} = \frac{-\frac{1}{a}\langle g(x), \psi^\star_{\mathbf{x},3,2,j}(\frac{x-b}{a})\rangle}{2\pi i\langle g(x), \psi^\star_{\mathbf{x},4,1,j}(\frac{x-b}{a})\rangle}, \tag{59}$$

for $j = -3, \ldots, 3$ (unless $(W_{\psi^\star_{\mathbf{x},4,1,j}}g)(a,b) = 0$), with $\psi_{\mathbf{x},3,2,j}$ and $\psi_{\mathbf{x},4,1,j}$ given in (57) and (56), respectively.

Lastly in this section, we describe the computation of $\mathcal{H}\psi_j$ in the construction of the analytic VM wavelets in (58). Since each $\psi_j = \psi_{\mathbf{x},4,1,j}$ is a linear combination of the B-splines $N_{\mathbf{x},4,-3}, \ldots, N_{\mathbf{x},4,4}$ [according to (56)], and since the Hilbert transform is translation invariant, the computation of $\mathcal{H}\psi_j$ consists in finding $\mathcal{H}N_{\mathbf{x},4,-3}, \ldots, \mathcal{H}N_{\mathbf{x},4,4}$. To this end, we recall the recurrence formula for the calculation of the cubic B-spline $N_{\mathbf{x},4,k}$, $k = -3, \ldots, 4$, in terms of lower order B-splines: for $\ell = 2, 3, 4$,

$$N_{\mathbf{x},\ell,k}(x) = \frac{x - x_k}{x_{\ell+k-1} - x_k} N_{\mathbf{x},\ell-1,k}(x) + \frac{x_{\ell+k} - x}{x_{\ell+k} - x_{k+1}} N_{\mathbf{x},\ell-1,k+1}(x),$$

with initial function $N_{\mathbf{x},1,k} := \chi_{[k,k+1)}$, the characteristic function on the interval $[k, k+1)$ (see de Boor 2001). It has been shown in Chen et al. (2006) that this relation is preserved by the Hilbert transform, so that, for $\ell = 2, 3, 4$,

$$(\mathcal{H}N_{\mathbf{x},\ell,k})(x) = \frac{x - x_k}{x_{\ell+k-1} - x_k}(\mathcal{H}N_{\mathbf{x},\ell-1,k})(x) + \frac{x_{\ell+k} - x}{x_{\ell+k} - x_{k+1}}(\mathcal{H}N_{\mathbf{x},\ell-1,k+1})(x),$$

with initial function

$$(\mathcal{H}N_{\mathbf{x},1,k})(x) = \frac{1}{\pi}\ln\left|\frac{x - x_k}{x - x_{k+1}}\right|.$$

This recurrence formulation may therefore be used to construct the analytic VM wavelets $\psi_j^\star = \psi_{\mathbf{x},4,1,j}^\star$, $j = -3, \ldots, 3$, in (58). The same procedure may be applied to obtain $\psi_{\mathbf{x},3,2,j}^\star$, required in (59).

5 Implementation and numerical experiments

Our proposed method of instantaneous frequency estimation of signal components can be summarized as follows:

1. Given a signal composed of a number of (not necessarily stationary) oscillating components, we apply EMD, equipped with our real-time cubic spline interpolation scheme, to separate the signal into its IMF components.
2. We apply the SST, with the analytic VM wavelet as analysis wavelet in the CWT, to each IMF separately to estimate its IF.
3. Lastly, we apply a smoothing spline curve fitting scheme, with automatic optimal smoothing parameter selection through generalized cross-validation, to the digital image produced by the SST to obtain the IF curve of a given IMF.

In practice, to apply this curve fitting scheme to the SST grayscale image, we proceed as follows.

Let S be the $\mu \times \nu$ output matrix of the SST, and let the entries in S be denoted by $p_{i,j}$ for $i = 1, \ldots, \mu$ and $j = 1, \ldots, \nu$. The entries $p_{i,j}$ may be interpreted as grayscale image pixel intensities, with the definition that an entry value of 0 represents a white pixel, and increasingly higher values represent increasingly darker pixels. (Note that pixels with a low intensity usually represent dark pixels in practice, while high intensity pixels usually represent light pixels. This setup is inverted in the above definition for application to the SST output matrix S.)

For each $j = 1, \ldots, \lfloor \frac{\nu}{n} \rfloor$, if

$$p_{nj}^* := \max\left\{p_{1,nj}, \ldots, p_{\mu,nj}\right\} > M,$$

where $M > 0$ (a thresholding parameter) and $n > 0$ (typically between 10 and 20) are chosen by the user, we record the row index of p_{nj}^* and denote this value by r_{nj} (so that $1 \leq r_{nj} \leq \mu$). Otherwise, we record the mean of the row indices of the pixel intensities higher than the 99th percentile of $\left\{p_{1,nj}, \ldots, p_{\mu,nj}\right\}$ and set this equal to r_{nj}.

Applying this process for each $j = 1, \ldots, \lfloor \frac{\nu}{n} \rfloor$, we obtain a sequence of ordered pairs $\left\{(r_n, n), \ldots, (r_{n\lfloor \nu/n \rfloor}, n\lfloor \frac{\nu}{n} \rfloor)\right\}$, to which we fit a smoothing spline curve with the optimal smoothing parameter determined through generalized cross-validation (see Wahba 1975; Craven and Wahba 1978; Golub et al. 1979; Carew et al. 2003).

We remark that the choice of using the 99th percentile of $p_{1,nj}, \ldots, p_{\mu,nj}$ as a thresholding parameter produces good results in practice, but it may be adjusted by the user.

We proceed to test our method on three representative signal types.

Our first test signal is a stationary signal with three components with integer frequencies, given by

$$f(t) = f_1(t) + f_2(t) + f_3(t), \tag{60}$$

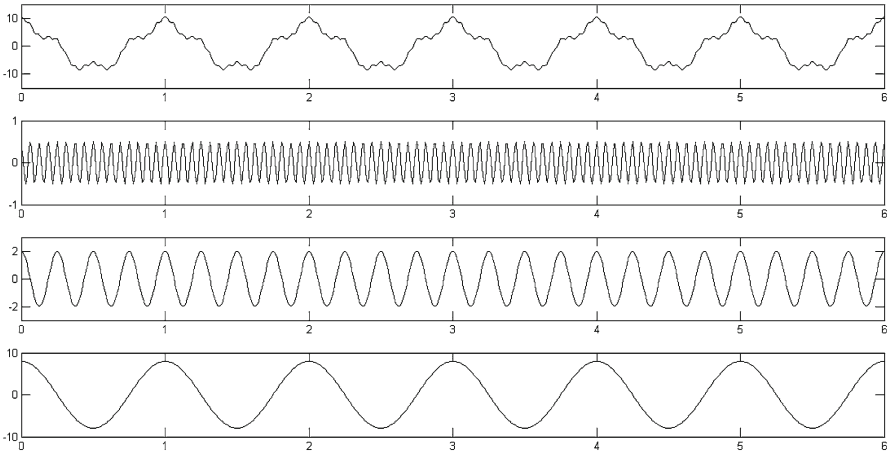

Fig. 4 *Top to bottom* original signal $f(t)$ and its components $f_1(t)$, $f_2(t)$, $f_3(t)$

where

$$f_1(t) = \tfrac{1}{2}\cos 2\pi(16t); \quad f_2(t) = 2\cos 2\pi(4t); \quad f_3(t) = 8\cos 2\pi t. \tag{61}$$

The signal f together with its three components are displayed in Fig. 4.

Figure 5 displays the three IMF's C_1, C_2 and C_3, approximating the components f_1, f_2 and f_3, respectively, constructed through applying EMD with our real-time cubic spline interpolation scheme. In Fig. 6, we illustrate the results of applying our modified SST (with the analytic VM wavelet of Sect. 4) to each IMF C_1, C_2 and C_3 obtained from the modified EMD. The SST digital image output is shown in grayscale in each case. The pixels selected for curve fitting are circled in red, and the resulting smoothing spline curve is shown as a red dashed line in each case. With the true IF's given by $\phi_2'(t) = 4$ and $\phi_3'(t) = 1$, the estimated IF's ϕ_2' and ϕ_3' in the second and third rows in Fig. 6 are very accurate. For the higher frequency component, the SST digital image in the first row of Fig. 6 displays a more noisy result, causing a lower estimated IF than the true value of 16, although it still reveals a constant frequency. We remark that greater noise reduction may be achieved by choosing an analytic VM wavelet with a higher number of vanishing moments (at the expense of computation time). The result here was obtained with an analytic VM wavelet with 5 vanishing moments (in terms of cubic B-splines so that $m = 4$).

Second, we test our method on another stationary signal with three components, two of which have irrational frequency values, given by

$$g(t) = g_1(t) + g_2(t) + g_3(t), \tag{62}$$

where

$$g_1(t) = \cos 2\pi(\sqrt{29}t); \quad g_2(t) = \cos 2\pi(\sqrt{13}t); \quad g_3(t) = \cos 2\pi t. \tag{63}$$

The signal g together with its three components are displayed in Fig. 7.

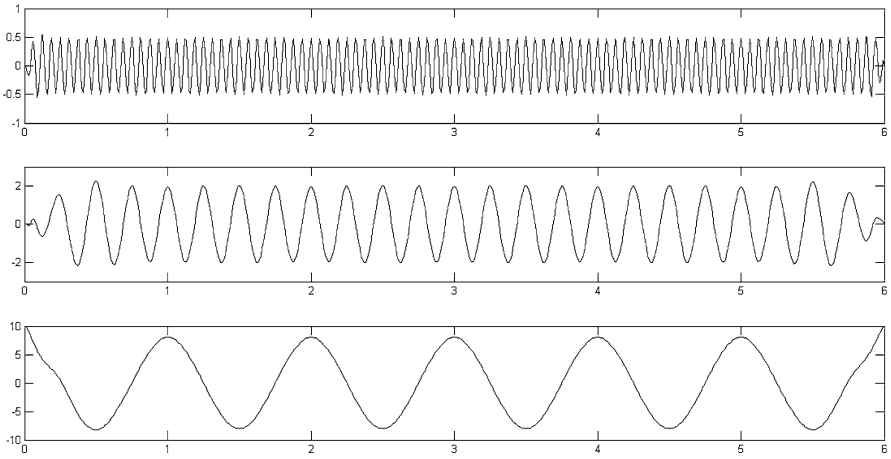

Fig. 5 First three IMF's C_1, C_2 and C_3 (*top to bottom*) constructed through applying EMD with our real-time cubic spline interpolation scheme

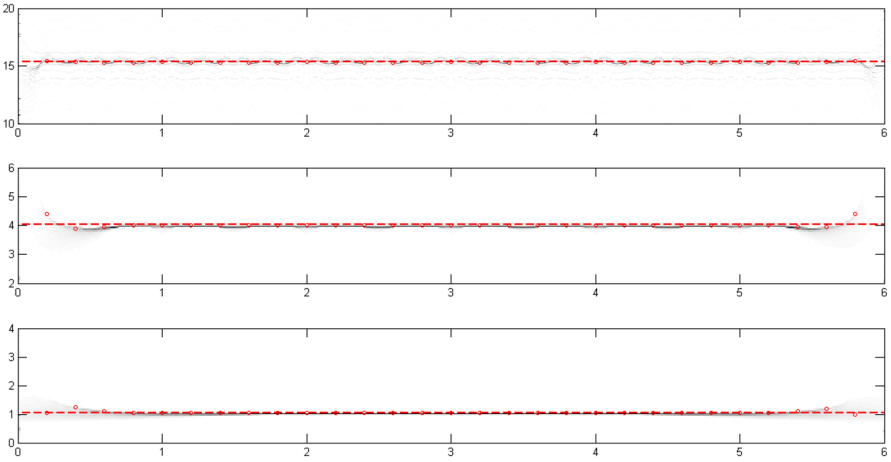

Fig. 6 The estimated IF's ϕ_1', ϕ_2' and ϕ_3' (*top to bottom*) of the IMF's C_1, C_2, C_3, respectively, graphed as the *red dashed line* in each case. The IF's are estimated from the digital image output of the SST applied to each IMF separately, shown in grayscale in each case, by fitting a smoothing spline curve through the pixels circled in *red*

Figure 8 displays the three IMF's C_1, C_2 and C_3, approximating the components g_1, g_2 and g_3, respectively, while Fig. 9 illustrates the results of applying our modified SST to each IMF C_1, C_2 and C_3, with the SST digital image output in grayscale, the pixels selected for curve fitting circled in red, and the resulting smoothing spline curve shown as a red dashed line in each case. The estimated IF's obtained through curve fitting applied to the SST digital image are remarkably accurate in each case.

Lastly, we implement our method for the non-linear, non-stationary signal with two components considered in Sect. 2, given by

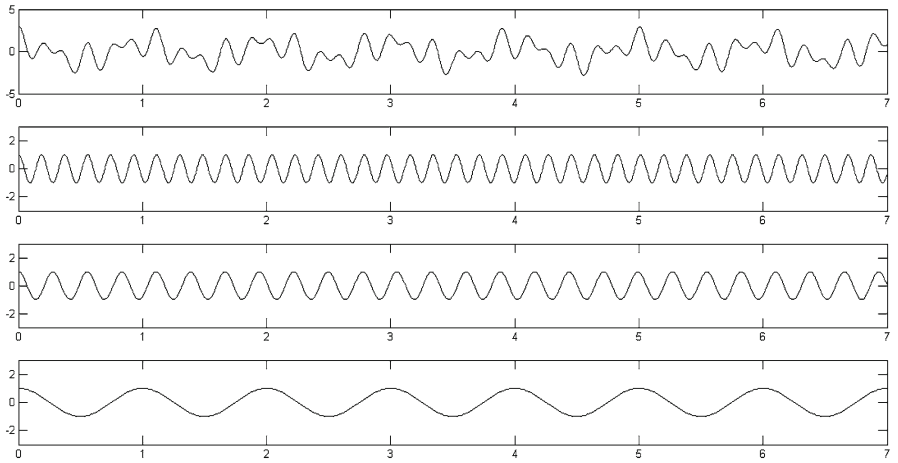

Fig. 7 *Top to bottom* original signal $g(t)$ and its components $g_1(t)$, $g_2(t)$, $g_3(t)$

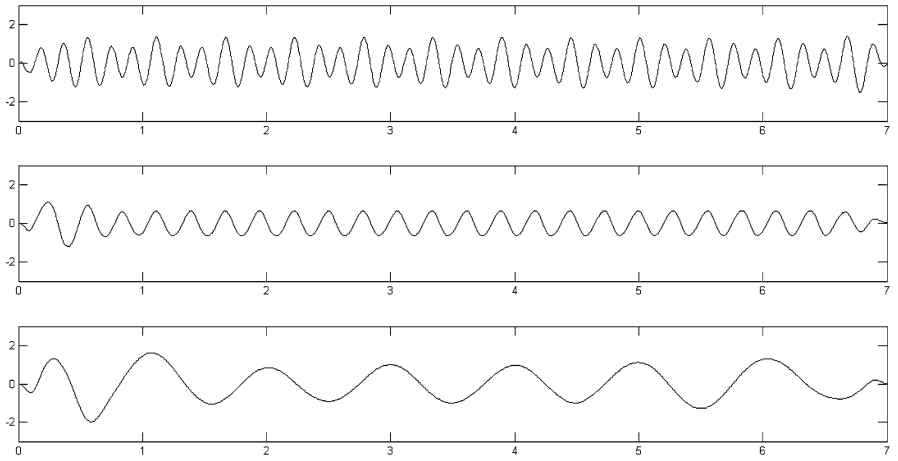

Fig. 8 First three IMF's C_1, C_2 and C_3 (*top to bottom*) constructed through applying EMD with our real-time cubic spline interpolation scheme

$$h(t) = h_1(t) + h_2(t), \tag{64}$$

where

$$\begin{cases} h_1(t) = 0.1(t^4 - 12t^3 + 44t^2 - 48t)\cos 2\pi(3t + 0.2t^2); \\ h_2(t) = e^{(-0.15t)}\cos 2\pi(2t + 0.2\cos t), \end{cases} \tag{65}$$

so that

$$\phi_1'(t) = 3 + 0.4t; \quad \phi_2'(t) = 2 - 0.2\sin t.$$

The signal h and its two components are shown in Fig. 10.

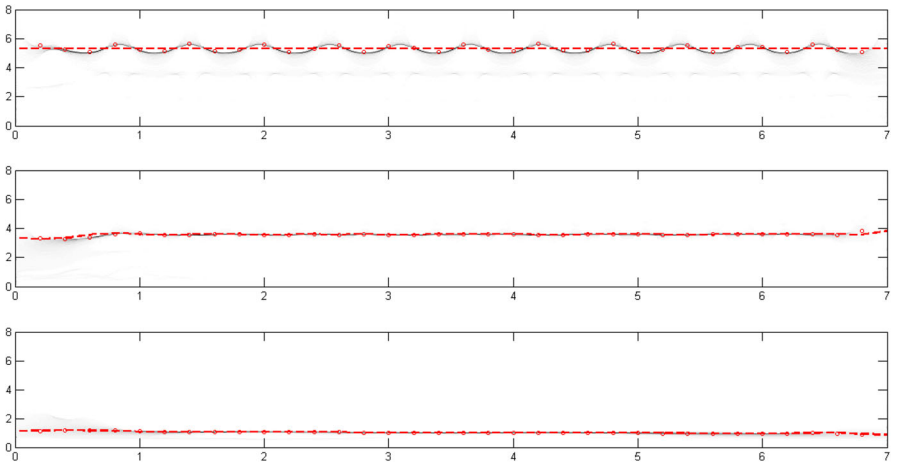

Fig. 9 The estimated IF's ϕ_1', ϕ_2' and ϕ_3' (*top to bottom*) of the IMF's C_1, C_2, C_3, respectively, graphed as the *red dashed line* in each case. The IF's are estimated from the digital image output of the SST applied to each IMF separately, shown in grayscale in each case, by fitting a smoothing spline curve through the pixels circled in *red*

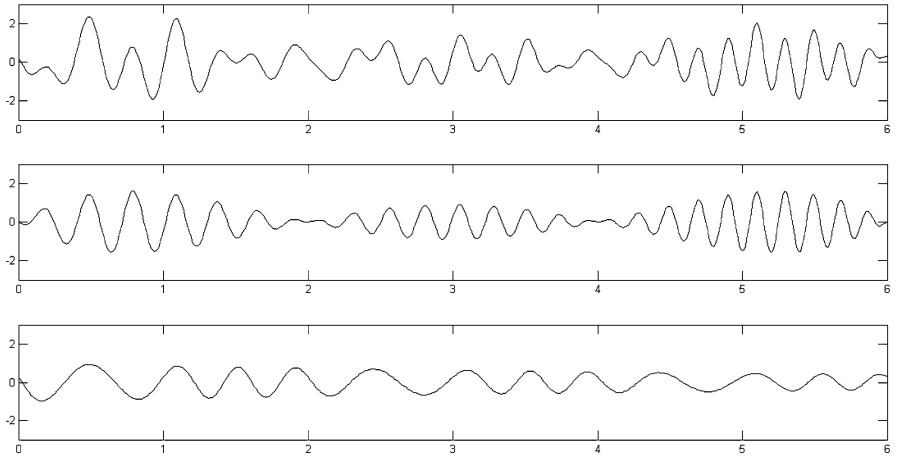

Fig. 10 *Top to bottom* original signal $h(t)$ and its components $h_1(t)$ and $h_2(t)$

Figure 11 displays the two IMF's C_1 and C_2, approximating the components h_1 and h_2, respectively, while Fig. 12 illustrates the results of applying our modified SST to each IMF C_1 and C_2, with the SST digital image output in grayscale, the pixels selected for curve fitting circled in red, and the resulting smoothing spline curve shown as a red dashed line in each case.

6 Proofs on blending operator construction

In this section, we provide proofs for Theorem 1, which states that the quasi-interpolation operator $\mathcal{Q}$ of Definition 1 preserves polynomials of degree ≤ 3, and

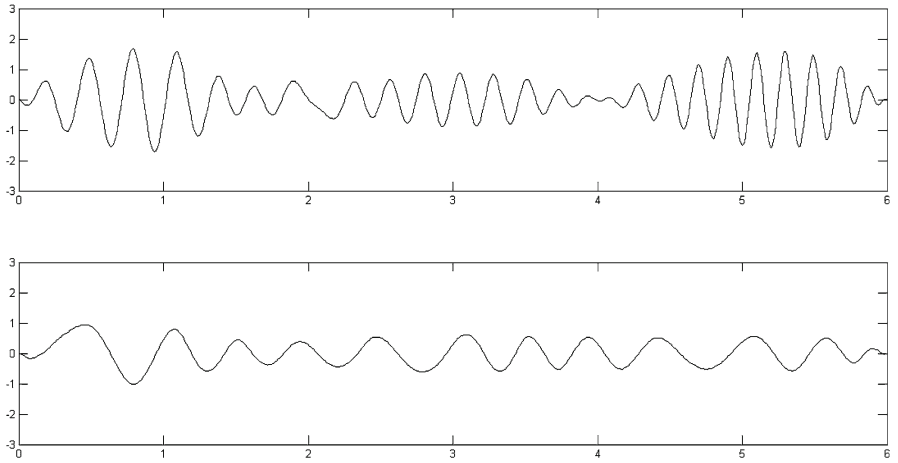

Fig. 11 First two IMF's C_1 and C_2 constructed through applying EMD with our real-time cubic spline interpolation scheme

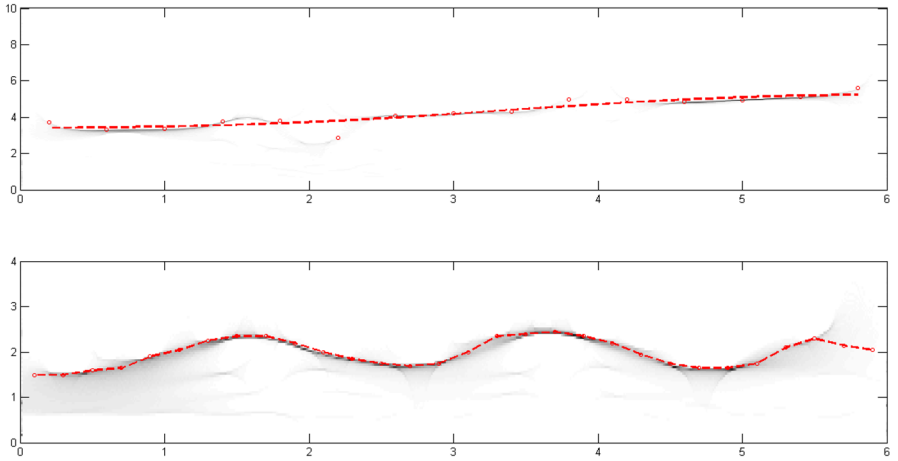

Fig. 12 The estimated IF's ϕ_1' and ϕ_2' of the IMF's C_1 and C_2, respectively, graphed as the *red dashed line* in each case. The IF's are estimated from the digital image output of the SST applied to each IMF separately, shown in grayscale in each case, by fitting a smoothing spline curve through the pixels circled in *red*

Theorem 3, which states that the blending operator $\mathcal{P}$ has a local formulation and satisfies the polynomial preservation property (25) and the Hermite interpolation conditions (26) and (27).

Proof of Theorem 1 We divide the proof into three parts.

(a) Let $x \in [x_6, x_{N-5}]$, so that (34) becomes simply

$$(\mathcal{Q}f)(x) = \sum_{i=3}^{N-3} f(x_i) M_i(x), \tag{66}$$

from the support properties of M_i in (41). We proceed to show that the constants $a_{i,j}, i = 3, \ldots, N-3,\ j = 0, 1, 2, 3$, satisfy the formulation (36) in Definition 1 if $\mathcal{Q}$ satisfies (42), for $p(x) = x^\ell,\ \ell = 0, 1, 2, 3$.
To this end, by using (66) and the second equation in (35), the left-hand side of (42) becomes

$$\begin{aligned}(\mathcal{Q}p)(x) &= \sum_{i=3}^{N-3} x_i^\ell \sum_{j=0}^{3} a_{i,j} N_{\mathbf{x},4,i+j-3}(x) \\ &= \sum_{j=0}^{3} \sum_{k=j}^{N-6+j} x_{k-j+3}^\ell a_{k-j+3,j} N_{\mathbf{x},4,k}(x) \\ &= \sum_{k=0}^{N-3} \sum_{j=\max\{0,k-N+6\}}^{\min\{3,k\}} x_{k-j+3}^\ell a_{k-j+3,j} N_{\mathbf{x},4,k}(x),\end{aligned} \tag{67}$$

for $p(x) = x^\ell,\ \ell = 0, 1, 2, 3$. Next, from Marsden's identity on the interval $[x_6, x_{N-5}]$, we have

$$x^\ell = \sum_{k=3}^{N-6} \xi^\ell(k) N_{\mathbf{x},4,k}(x), \quad \ell = 0, 1, 2, 3, \tag{68}$$

where ξ^ℓ is defined in terms of the classical symmetric functions as in (31), (32) and (33). By substituting (67) and (68) in (42), we obtain

$$\sum_{j=\max\{0,k-N+6\}}^{\min\{3,k\}} x_{k-j+3}^\ell a_{k-j+3,j} = \xi^\ell(k), \quad \ell = 0, 1, 2, 3,$$

for $k = 3, \ldots, N-6$, yielding (for $N \geq 9$)

$$\sum_{j=0}^{3} x_{k-j+3}^\ell a_{k-j+3,j} = \xi^\ell(k), \quad \ell = 0, 1, 2, 3.$$

The formulation (36) in Definition 1 then follows by using Cramer's rule.

(b) Next, let $x \in [a, x_6]$, so that (34) becomes

$$(\mathcal{Q}f)(x) = \sum_{\ell=1}^{3} f^{(\ell)}(x_0) M_{-\ell}(x) + \sum_{i=0}^{8} f(x_i) M_i(x), \tag{69}$$

from the support properties of M_i in (41). As in the first part, we show that the constants $a_{i,j}$, $i = -3, \ldots, 2$, satisfy the formulation (36), (37), (38) in Definition 1 if $\mathcal{Q}$ satisfies (42), for $p(x) = x^\ell$, $\ell = 0, 1, 2, 3$.
By using (69) and the first two equations in (35), the left-hand side of (42) becomes

$$\begin{aligned}
(\mathcal{Q}p)(x) &= (\ell)(\ell-1)(\ell-2)x_0^{\ell-3}a_{-3,0}N_{\mathbf{x},4,-3}(x) \\
&\quad +(\ell)(\ell-1)x_0^{\ell-2}\sum_{j=0}^{1}a_{-2,j}N_{\mathbf{x},4,j-3}(x) \\
&\quad +\ell x_0^{\ell-1}\sum_{j=0}^{2}a_{-1,j}N_{\mathbf{x},4,j-3}(x) \\
&\quad +\sum_{i=0}^{8}x_i^\ell\sum_{j=0}^{3}a_{i,j}N_{\mathbf{x},4,i+j-3}(x) \\
&= (\ell)(\ell-1)(\ell-2)x_0^{\ell-3}a_{-3,0}N_{\mathbf{x},4,-3}(x) \\
&\quad +\sum_{k=-3}^{-2}(\ell)(\ell-1)x_0^{\ell-2}a_{-2,k+3}N_{\mathbf{x},4,k}(x) \\
&\quad +\sum_{k=-3}^{-1}\ell x_0^{\ell-1}a_{-1,k+3}N_{\mathbf{x},4,k}(x) \\
&\quad +\sum_{j=0}^{3}\sum_{k=j-3}^{j+5}x_{k-j+3}^{\ell}a_{k-j+3,j}N_{\mathbf{x},4,k}(x) \\
&= (\ell)(\ell-1)(\ell-2)x_0^{\ell-3}a_{-3,0}N_{\mathbf{x},4,-3}(x) \\
&\quad +\sum_{k=-3}^{-2}(\ell)(\ell-1)x_0^{\ell-2}a_{-2,k+3}N_{\mathbf{x},4,k}(x) \\
&\quad +\sum_{k=-3}^{-1}\ell x_0^{\ell-1}a_{-1,k+3}N_{\mathbf{x},4,k}(x) \\
&\quad +\sum_{k=-3}^{8}\sum_{j=\max\{0,k-5\}}^{\min\{3,k+3\}}x_{k-j+3}^{\ell}a_{k-j+3,j}N_{\mathbf{x},4,k}(x). \qquad (70)
\end{aligned}$$

Combining (42) and (70) with Marsden's identity on the interval $[a, x_6]$, namely

$$x^\ell = \sum_{k=-3}^{5}\xi^\ell(k)N_{\mathbf{x},4,k}(x), \quad \ell = 0, 1, 2, 3,$$

we have

$$\begin{aligned}
&\Big[\ell(\ell-1)(\ell-2)x_0^{\ell-3}a_{-3,0}+\ell(\ell-1)x_0^{\ell-2}a_{-2,0}+\ell x_0^{\ell-1}a_{-1,0}\\
&\quad +x_0^{\ell}a_{0,0}\Big]N_{\mathbf{x},4,-3}(x)\\
&+\left[\ell(\ell-1)x_0^{\ell-2}a_{-2,1}+\ell x_0^{\ell-1}a_{-1,1}+\sum_{j=0}^{1}x_{1-j}^{\ell}a_{1-j,j}\right]N_{\mathbf{x},4,-2}(x)\\
&+\left[\ell x_0^{\ell-1}a_{-1,2}+\sum_{j=0}^{2}x_{2-j}^{\ell}a_{2-j,j}\right]N_{\mathbf{x},4,-1}(x)\\
&+\sum_{k=0}^{2}\left[\sum_{j=0}^{3}x_{k-j+3}^{\ell}a_{k-j+3,j}\right]N_{\mathbf{x},4,k}(x)=\sum_{k=-3}^{2}\xi^{\ell}(k)N_{\mathbf{x},4,k}(x).
\end{aligned}$$

The result follows by comparing the left hand side and right hand side for $k = -3, \ldots, 2$, and using Cramer's rule. The formulation (36) corresponds to $k = 0, 1, 2$, while (37) and (38) (in terms of confluent Vandermonde determinants) correspond to $k = -3, -2, -1$.

(c) Lastly, when $x \in [x_{N-5}, b]$, we obtain the coefficients in (36), (39) and (40) under the requirement that $\mathcal{Q}$ satisfies (42). The proof follows a similar pattern as the proof in part (b) above. □

Using Theorems 1 and 2, we may prove Theorem 3.

Proof of Theorem 3 (i) Firstly, from (48), (49) and the support properties (41) and (46), it is clear that $\mathcal{P}$ is local.

(ii) To show the polynomial preservation property (25), let p be a polynomial in π_3. Then, from Theorem 1,

$$\begin{aligned}
(\mathcal{P}p)(x) &= (\mathcal{Q}p)(x)+(\mathcal{R}p)(x)-(\mathcal{R}(\mathcal{Q}p))(x)\\
&= p(x)+(\mathcal{R}p)(x)-(\mathcal{R}p)(x)=p(x),
\end{aligned}$$

for all $x \in [a, b]$.

(iii) To show that $\mathcal{P}f$ interpolates f at x_i, $i = 0, \ldots, N+1$, we may use Theorem 2 together with (43), (47) and (45) to deduce that

$$\begin{aligned}
(\mathcal{P}f)(x_i) &= (\mathcal{Q}f)(x_i)+(\mathcal{R}f)(x_i)-(\mathcal{R}(\mathcal{Q}f))(x_i)\\
&= (\mathcal{Q}f)(x_i)+f(x_i)-(\mathcal{Q}f)(x_i)=f(x_i),
\end{aligned}$$

for $i = 0, \ldots, N+1$, yielding (26).

(iv) Lastly, we observe that

$$\begin{aligned}
(\mathcal{R}(\mathcal{Q}f))^{(n)}(x_0) &= (\mathcal{Q}f)^{(n)}(x_0); \quad n=1,2,3;\\
(\mathcal{R}(\mathcal{Q}f))^{(n)}(x_{N+1}) &= (\mathcal{Q}f)^{(n)}(x_{N+1}), \quad n=1,2,
\end{aligned}$$

from the construction of $\mathcal{R}$ and the spline molecules L_i in Definition 2. Therefore, using also Theorem 2, we have

$$\begin{aligned}(\mathcal{P}f)^{(n)}(x_0) &= (\mathcal{Q}f)^{(n)}(x_0) + (\mathcal{R}f)^{(n)}(x_0) - (\mathcal{R}(\mathcal{Q}f))^{(n)}(x_0)\\ &= (\mathcal{Q}f)^{(n)}(x_0) + f^{(n)}(x_0) - (\mathcal{Q}f)^{(n)}(x_0) = f^{(n)}(x_0),\end{aligned}$$

for $n = 1, 2, 3$, and

$$\begin{aligned}(\mathcal{P}f)^{(n)}(x_{N+1}) &= (\mathcal{Q}f)^{(n)}(x_{N+1}) + (\mathcal{R}f)^{(n)}(x_{N+1}) - (\mathcal{R}(\mathcal{Q}f))^{(n)}(x_{N+1})\\ &= (\mathcal{Q}f)^{(n)}(x_{N+1}) + f^{(n)}(x_{N+1}) - (\mathcal{Q}f)^{(n)}(x_{N+1})\\ &= f^{(n)}(x_{N+1}),\end{aligned}$$

for $n = 1, 2$, so that (27) follows. □

7 Comparison of methods

We now turn our attention to graphically comparing our hybrid EMD-SST computational scheme with the original EMD-HSA approach. To this end, we apply the two methods to the three signals considered in Sect. 5.

In Fig. 13, we compare the construction of IMF's through the two methods for the first test signal $f(t)$ defined in (60), (61). The true components $f_1(t)$, $f_2(t)$ and $f_3(t)$ are shown in the left hand side column. The middle column displays the IMF's $C_1^O(t)$, $C_2^O(t)$ and $C_3^O(t)$ constructed through the original EMD algorithm using standard cubic spline interpolation in the sifting process, while the right hand side column shows the IMF's $C_1^S(t)$, $C_2^S(t)$ and $C_3^S(t)$ obtained by applying the modified EMD using our real-time cubic spline interpolation scheme in the sifting process. The results are comparable for the first two components; however, our real-time interpolation scheme produces a closer approximation of the third component, especially close to the boundaries.

A comparison of the estimated IF's is given in Fig. 14. The column on the left displays the true IF's $\phi_1'(t) = 16$, $\phi_2'(t) = 4$ and $\phi_3'(t) = 1$. The middle column displays the estimated IF's $\phi_1'^O(t)$, $\phi_2'^O(t)$ and $\phi_3'^O(t)$, obtained by applying Hilbert spectral analysis to each IMF C_j^O, $j = 1, 2, 3$. On the right we show our estimated IF's $\phi_1'^S(t)$, $\phi_2'^S(t)$ and $\phi_3'^S(t)$, constructed through smoothing spline curve fitting (with generalized cross-validation) to our modified SST applied to each C_j^S, $j = 1, 2, 3$ separately. Our hybrid EMD-SST method yield better results than the original EMD-HSA approach close to the boundaries. Although our estimation $\phi_1'^S$ shows a constant frequency, it is a bit lower than the true value of 16. As explained in Sect. 5, this could be improved upon by implementing an analysis wavelet with a higher number of vanishing moments.

In Fig. 15, we compare the construction of IMF's for the signal $g(t)$ defined in (62), (63). The true components $g_1(t)$, $g_2(t)$ and $g_3(t)$ are shown in the left hand side column. The middle column displays the IMF's $C_1^O(t)$, $C_2^O(t)$ and $C_3^O(t)$ constructed

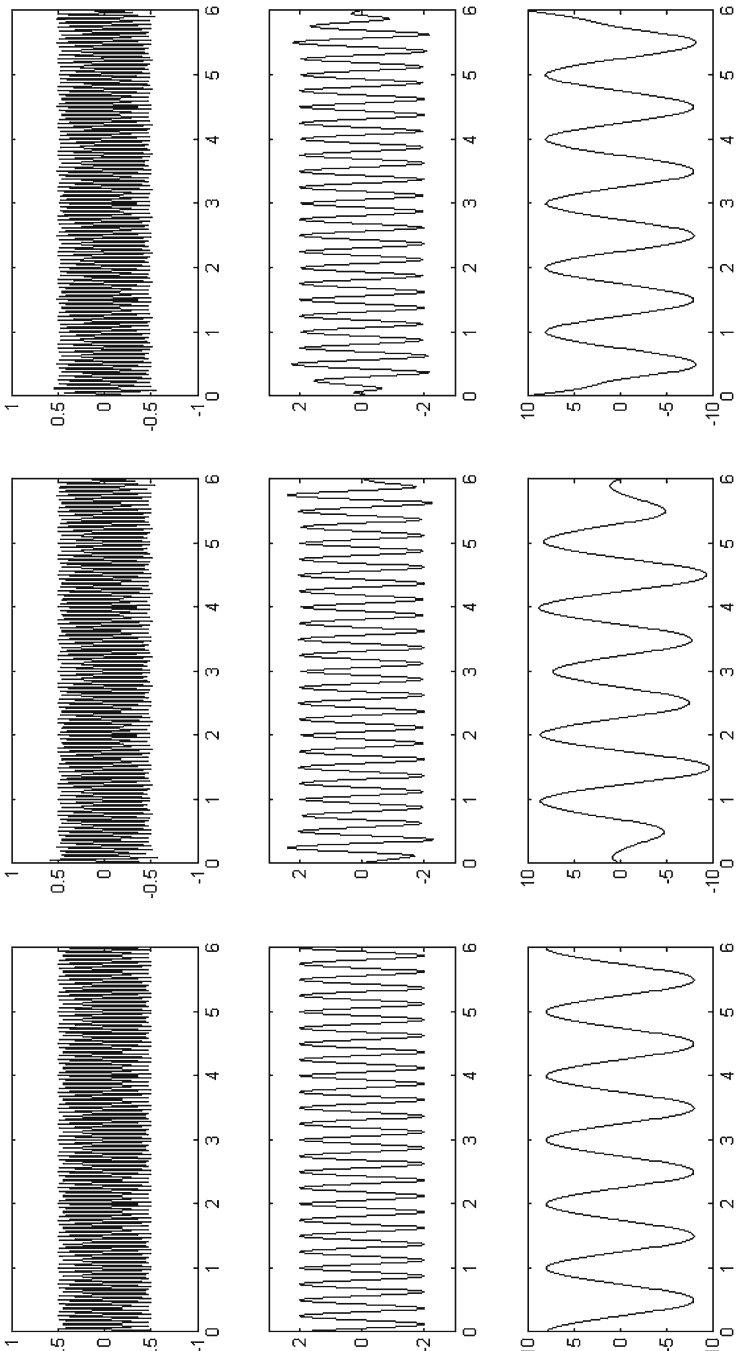

Fig. 13 *Left* true components f_1, f_2, f_3 (*top to bottom*); *middle* IMF's C_1^O, C_2^O, C_3^O (*top to bottom*) obtained from the original EMD with standard cubic spline interpolation; *right* IMF's C_1^S, C_2^S, C_3^S (*top to bottom*) obtained through applying EMD with our real-time cubic spline interpolation scheme

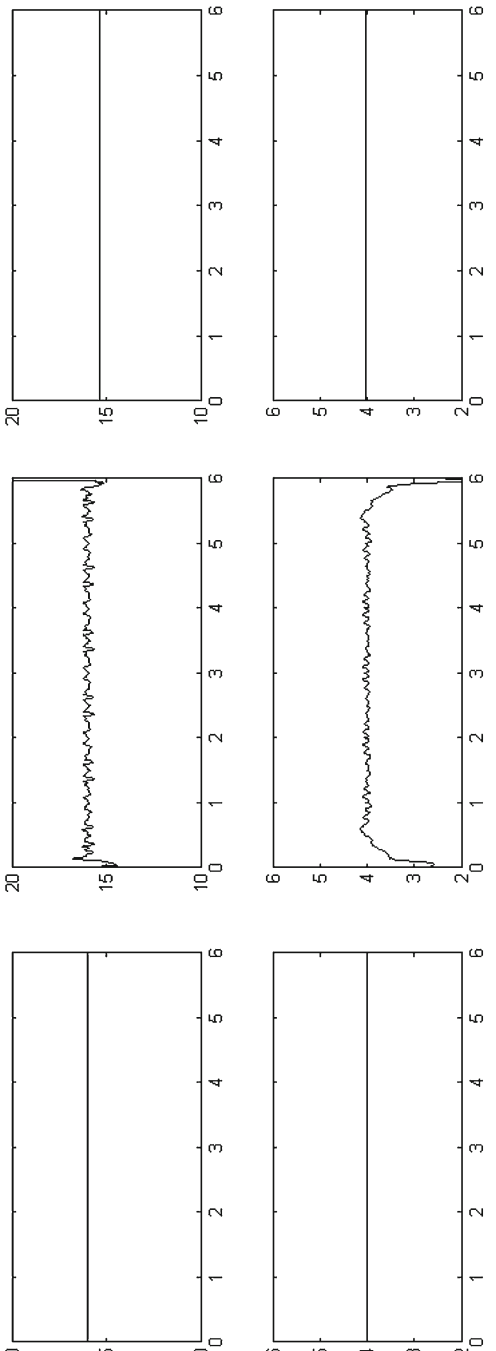

Fig. 14 *Left* true IF's ϕ_1', ϕ_2', ϕ_3' (*top to bottom*); *middle* estimated IF's $\phi_1'^O$, $\phi_2'^O$, $\phi_3'^O$ (*top to bottom*) obtained by applying HSA to the original EMD; *right* estimated IF's $\phi_1'^S$, $\phi_2'^S$, $\phi_3'^S$ (*top to bottom*) obtained through smoothing spline curve fitting of our modified SST applied to each IMF C_j^S, $j = 1, 2, 3$ separately

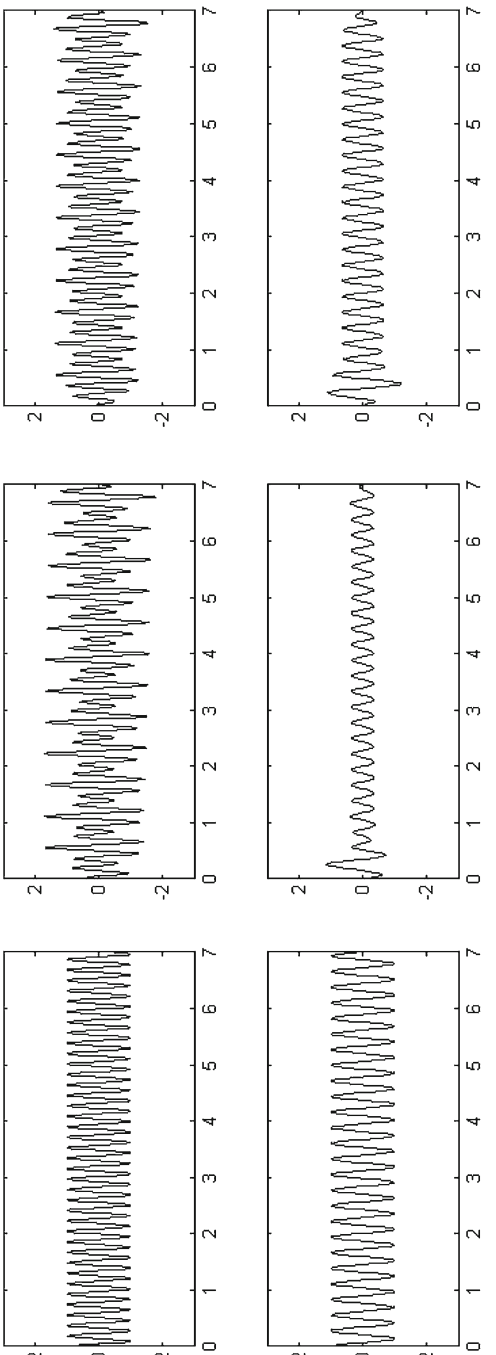

Fig. 15 *Left* true components g_1, g_2, g_3 (*top to bottom*); *middle* IMF's C_1^O, C_2^O, C_3^O (*top to bottom*) obtained from the original EMD with standard cubic spline interpolation; *right* IMF's C_1^S, C_2^S, C_3^S (*top to bottom*) obtained through applying EMD with our real-time cubic spline interpolation scheme

through the original EMD algorithm using standard cubic spline interpolation, while the right hand side column shows the IMF's $C_1^S(t)$, $C_2^S(t)$ and $C_3^S(t)$ obtained by applying the modified EMD using our real-time cubic spline interpolation scheme. Our method provides a better approximation of especially the first and second components (rows 1 and 2).

A comparison of the estimated IF's is given in Fig. 16. The column on the left displays the true IF's $\phi_1'(t) = \sqrt{29} \approx 5.385$, $\phi_2'(t) = \sqrt{13} \approx 3.606$ and $\phi_3'(t) = 1$. The middle column displays the estimated IF's $\phi_1'^O(t)$, $\phi_2'^O(t)$ and $\phi_3'^O(t)$, obtained by applying Hilbert spectral analysis to each IMF C_j^O, $j = 1, 2, 3$. On the right we show our estimated IF's $\phi_1'^S(t)$, $\phi_2'^S(t)$ and $\phi_3'^S(t)$, constructed through smoothing spline curve fitting (with generalized cross-validation) and our modified SST applied to each C_j^S, $j = 1, 2, 3$ separately. Our hybrid EMD-SST scheme yield much better estimations of all three IF's $\phi_1'(t)$, $\phi_2'(t)$ and $\phi_3'(t)$ than the original EMD-HSA approach.

In Fig. 17, we compare the construction of IMF's for the non-stationary signal $h(t)$, defined in (64), (65). The true components $h_1(t)$ and $h_2(t)$ are shown in the left hand side column. The middle column displays the IMF's $C_1^O(t)$ and $C_2^O(t)$ constructed through the original EMD algorithm using standard cubic spline interpolation in the sifting process, while the right hand side column shows the IMF's $C_1^S(t)$ and $C_2^S(t)$ obtained by applying the modified EMD using our real-time cubic spline interpolation scheme in the sifting process. Our method yield somewhat more accurate approximations of both signal components.

Lastly, a comparison of the estimated IF's is given in Fig. 18. The column on the left displays the true IF's $\phi_1'(t) = 3 + 0.4t$ and $\phi_2'(t) = 2 - 0.2 \sin t$. The middle column displays the estimated IF's $\phi_1'^O(t)$ and $\phi_2'^O(t)$, obtained by applying Hilbert spectral analysis to each IMF C_j^O, $j = 1, 2$. On the right we show our estimated IF's $\phi_1'^S(t)$ and $\phi_2'^S(t)$, constructed through smoothing spline curve fitting (with generalized cross-validation) and our modified SST applied to each C_j^S, $j = 1, 2$ separately. Our hybrid EMD-SST provide much better estimations of the IF's of both signal components.

8 Final remarks

In this paper, the sifting process of the EMD scheme is used to decompose a given signal f, by applying our local cubic spline interpolation of local maxima and local minima. In a nutshell, while the first signal component f_1 of f is obtained by subtracting a certain cubic spline function s_1 from f, the remaining signal components, $f_k = s_{k-1} - s_k$, for $k = 2, \ldots, K$, are cubic spline functions, where s_k is based on cubic spline interpolation of the local extrema of the previous cubic spline s_{k-1}. Hence, the decomposition of f into its signal components $f_1, \ldots, f_K$ may be viewed as *waveform-based decomposition*. Observe that the frequency content of each f_k is inherited from the alternate neighboring local maxima and minima.

On the other hand, the popular signal decomposition schemes using wavelets and/or wavelet-packets are based mainly on frequency bands (in terms of multi-level scales), without direct consideration of waveforms. Therefore it is inconceivable that wavelet

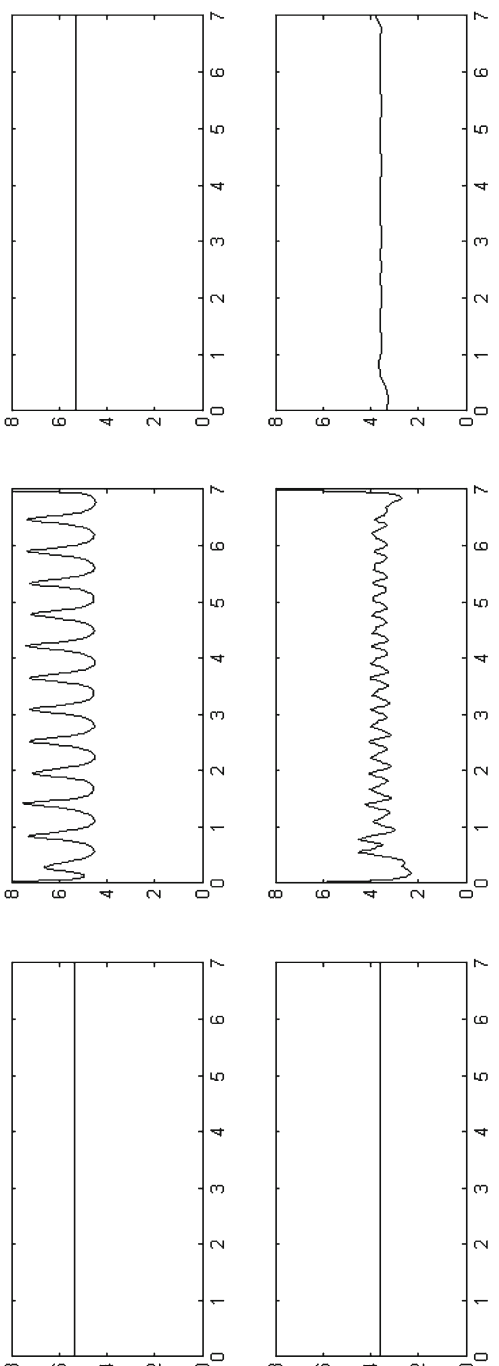

Fig. 16 *Left* true IF's ϕ_1', ϕ_2', ϕ_3' (*top to bottom*); *middle* estimated IF's $\phi_1'^O$, $\phi_2'^O$, $\phi_3'^O$ (*top to bottom*) obtained by applying HSA to the original EMD; *right* estimated IF's $\phi_1'^S$, $\phi_2'^S$, $\phi_3'^S$ (*top to bottom*) obtained through smoothing spline curve fitting of our modified SST applied to each IMF C_j^S, $j = 1, 2, 3$ separately

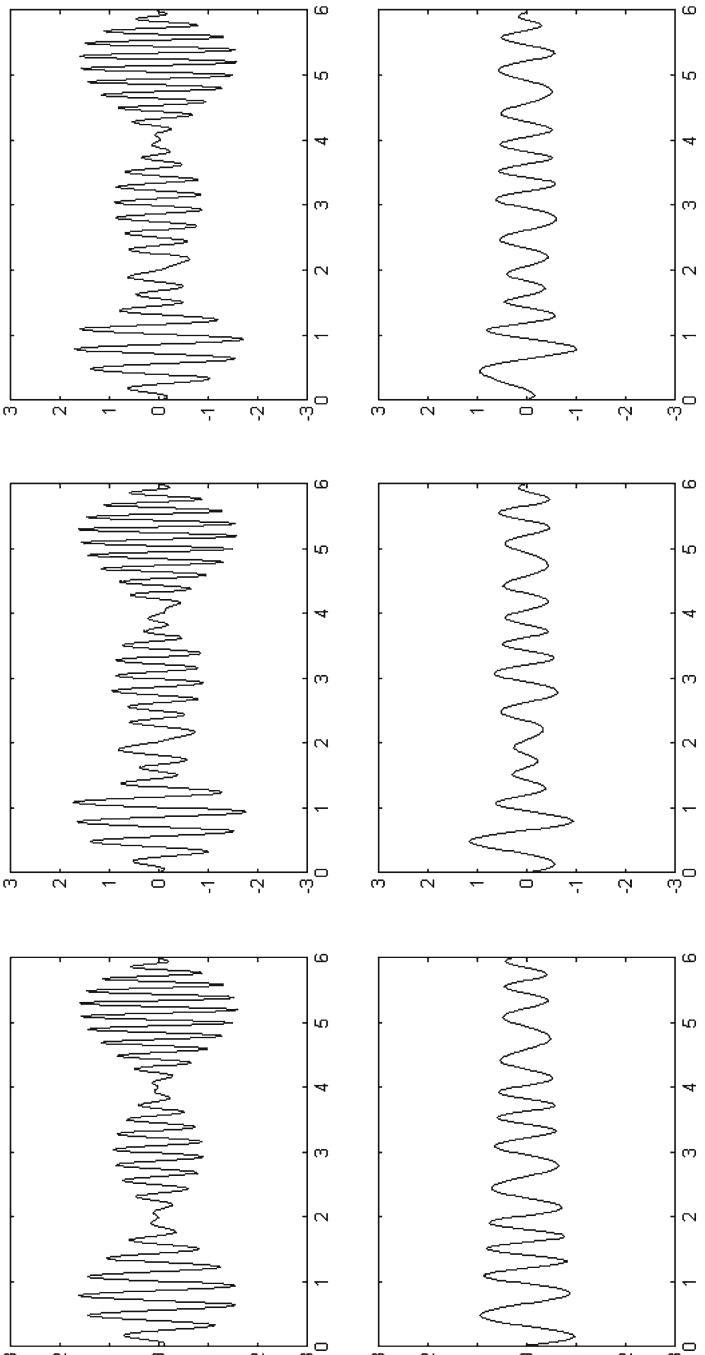

Fig. 17 *Left* true components h_1, h_2 (*top to bottom*); *middle* IMF's C_1^O, C_2^O (*top to bottom*) obtained from the original EMD with standard cubic spline interpolation; *right* IMF's C_1^S, C_2^S (*top to bottom*) obtained through applying EMD with our real-time cubic spline interpolation scheme

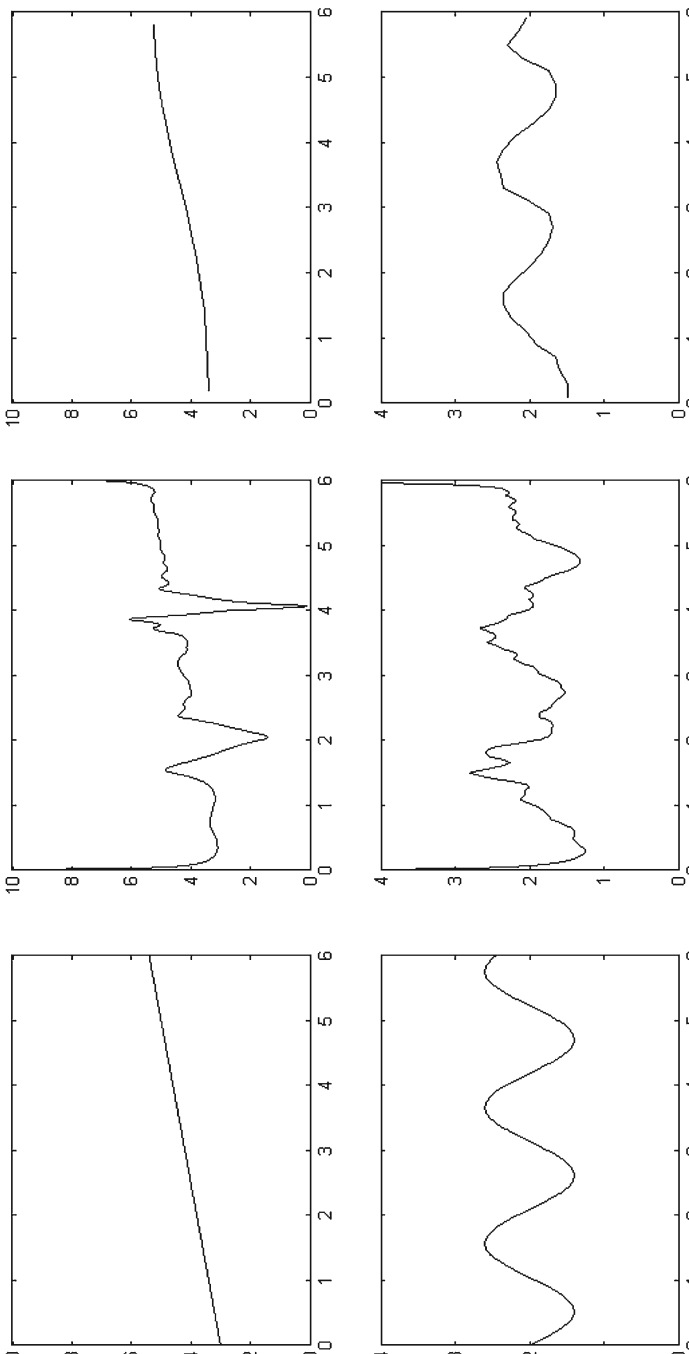

Fig. 18 *Left* true IF's ϕ_1', ϕ_2' (*top to bottom*); *middle* estimated IF's $\phi_1'^O$, $\phi_2'^O$ (*top to bottom*) obtained by applying HSA to the original EMD; *Right* estimated IF's $\phi_1'^S$, $\phi_2'^S$ (*top to bottom*) obtained through smoothing spline curve fitting of our modified SST applied to each IMF C_j^S, $j = 1, 2$ separately

decomposition could be applied to compute the signal components from a blind source signal in AHM. For example, let us consider the blind source

$$f(t) = \cos 2\pi t + a \cos 2\pi \omega t, \quad a > 0,\ 0 < \omega < 1, \tag{71}$$

with two (unknown) frequencies 1 and ω, as considered in Wu et al. (2011). When a wavelet decomposition scheme is applied to f in (71), it is necessary to iterate significantly over 2 times to yield a slowly oscillating remainder, for any choice of bi-orthogonal wavelet filter pair. Hence, there would be over two signal components and instantaneous frequencies at each time instant t.

As mentioned in the introduction, the EMD scheme is not designed to separate a blind source signal into specific components of the model AHM either. For instance, the EMD is not capable of separating the blind source f in (71) at all for $0.75 < \omega < 1$ (Rilling and Flandrin 2008).

When certain specifications are imposed on the AHM, the SST method can be applied directly, without EMD, to identify the frequency $\omega = 0.70$, but fails for $0.90 \leq \omega < 1$ (see Fig. 5 in Wu et al. 2011). On the other hand, under somewhat less restrictive conditions, the direct method introduced in Chui and Mhaskar (2015) is capable of finding the two (unknown) frequencies 1 and ω, even for $\omega = 0.99$. In a forthcoming paper, we will replace SST by this direct method for our hybrid approach without imposing any specifications on the AHM. This is feasible, since the signal restrictions in Chui and Mhaskar (2015) are mainly for finding the number K of signal components of the AHM and separating the instantaneous frequencies. These requirements are no longer necessary in view of our modified and improved sifting process.

Acknowledgments The research of Charles K. Chui was supported by ARO Grant # W911 NF-11-1-0426.

References

Boashash, B.: Estimating and interpreting the instantaneous frequency of a signal. i. Fundamentals. Proc. IEEE **80**(4), 520–538 (1992)

Boashash, B.: Estimating and interpreting the instantaneous frequency of a signal. ii. Algorithms and applications. Proc. IEEE **80**(4), 540–568 (1992)

Carew, J.D., Wahba, G., Xie, X., Nordheim, E.V., Elizabeth Meyerand, M.: Optimal spline smoothing of fmri time series by generalized cross-validation. NeuroImage **18**(4), 950–961 (2003)

Chen, G., Chui, Charles K., Lai, M.J.: Construction of real-time spline quasi-interpolation schemes. Approx. Theory Appl. **4**(4), 61–75 (1988)

Chen, Q., Huang, N.E., Riemenschneider, S., Xu, Y.: A B-spline approach for empirical mode decompositions. Adv. Comput. Math. **24**(1–4), 171–195 (2006)

Chen, Y.-C., Cheng, M.-Y., Wu, H.-T.: Non-parametric and adaptive modelling of dynamic periodicity and trend with heteroscedastic and dependent errors. J. Roy. Stat. Soc. Ser. B (Stat. Methodol.) **76**(3), 651–682 (2014)

Chui, C.K., Mhaskar, H.N.: Signal decomposition and analysis via extraction of frequencies. Appl. Comput. Harmon. Anal. (2015). http://dx.doi.org/10.1016/j.acha.2015.01.003

Chui, C.K., Diamond, H.: A general framework for local interpolation. Numerische Mathematik **58**(1), 569–581 (1990)

Chui, C.K., Lin, Y.-T., Wu, H.-T.: Real-time dynamics acquisition from irregular samples—with application to anesthesia evaluation. arXiv preprint arXiv:1406.1276 (2014)

Craven, P., Wahba, G.: Smoothing noisy data with spline functions. Numerische Mathematik **31**(4), 377–403 (1978)
Curry, H.B., Schoenberg, I.J.: On Pólya frequency functions iv: The fundamental spline functions and their limits. Journal d'Analyse Math-matique **17**(1), 71–107 (1966)
Daubechies, I., Lu, J., Wu, H.-T.: Synchrosqueezed wavelet transforms: an empirical mode decomposition-like tool. Appl. Comput. Harmon. Anal. **30**, 243–261 (2011)
Daubechies, I., Maes, S.: A nonlinear squeezing of the continuous wavelet transform based on auditory nerve models. In: Aldroubi, A., Unser, M.A. (eds.) Wavelets in Medicine and Biology, pp. 527–546. CRC Press, Boca Raton (1996)
de Boor, C.: A Practical Guide to Splines. Applied Mathematical Sciences, vol. 27. Springer, Berlin (2001)
de Boor, C., Fix, G.: Spline approximation by quasi-interpolants. J. Approx. Theory **8**, 96–110 (1973)
Gabor, D.: Theory of communication. J. Inst. Electr. Eng. Part III Radio Commun. Eng. **93**(26), 429–441 (1946)
Golub, G.H., Heath, M., Wahba, G.: Generalized cross-validation as a method for choosing a good ridge parameter. Technometrics **21**(2), 215–223 (1979)
Heisenberg, W.: Über den anschaulichen Inhalt der quantentheoretischen Kinematik und Mechanik. Zeitschrift für Physik **43**(3–4), 172–198 (1927)
Huang, N.E., Shen, Z., Long, S.R., Wu, M.C., Shih, H.H., Zheng, Q., Yen, N.-C., Tung, C.C., Liu, H.H.: The empirical mode decomposition and the Hilbert spectrum for nonlinear and non-stationary time series analysis. Proc. Roy. Soc. Lond. Ser. A Math. Phys. Eng. Sci. **454**(1971), 903–995 (1998)
Huang, N.E., Wu, Z.: A review on Hilbert-Huang transform: method and its applications to geophysical studies. Rev. Geophys. **46**(2), 1–23 (2008)
Kennard, E.H.: Zur Quantenmechanik einfacher Bewegungstypen. Zeitschrift für Physik **44**(4–5), 326–352 (1927)
Rilling, G., Flandrin, P.: One or two frequencies? the empirical mode decomposition answers. IEEE Trans. Signal Process. **56**(1), 85–95 (2008)
Sharpley, R.C., Vatchev, V.: Analysis of the intrinsic mode functions. Constr. Approx. **24**(1), 17–47 (2006)
Thakur, G., Wu, H.-T.: Synchrosqueezing-based recovery of instantaneous frequency from nonuniform samples. SIAM J. Math. Anal. **43**(5), 2078–2095 (2011)
Van der Pol, B.: The fundamental principles of frequency modulation. J. Inst. Electr. Eng. Part III Radio Commun. Eng. **93**(23), 153–158 (1946)
Wahba, G.: Smoothing noisy data with spline functions. Numerische Mathematik **24**(5), 383–393 (1975)
Weyl, H.: Gruppentheorie und Quantenmechanik (1928)
Wu, H.-T., Flandrin, P., Daubechies, I.: One or two frequencies? The synchrosqueezing answers. Adv. Adapt. Data Anal. **3**(01n02), 29–39 (2011)
Wu, Z., Huang, N.E.: A study of the characteristics of white noise using the empirical mode decomposition method. Proc. Roy. Soc. Lond. Ser. A Math. Phys. Eng. Sci. **460**(2046), 1597–1611 (2004)
Wu, Z., Huang, N.E.: Ensemble empirical mode decomposition: a noise-assisted data analysis method. Adv. Adap. Data Anal. **1**(01), 1–41 (2009)